Facies (2024) 70:7
https://doi.org/10.1007/s10347-024-00681-2

ORIGINAL ARTICLE

Evolution of coniacian facies and environments in the Iberian basin: a longshore current controlling siliciclastic sand distribution on a carbonate platform

J. Gil-Gil[1] · A. Bretones[1] · C. Boix[1] · J. F. García-Hidalgo[1]

Received: 21 September 2023 / Accepted: 21 February 2024

Abstract

The Coniacian carbonate sediments of the Iberian basin were deposited on a homoclinal ramp that grades upwards into a distally steepened ramp, with a major shoreline siliciclastic fringe. Twenty-three facies have been identified and grouped into three main depositional environments: outer, mid, and inner ramp. The last include barrier (shoal), lagoon, carbonate tidal-flat and shoreface sub-environments. The more prominent biogenic components show a mixture of sunlight-dependent phototrophic organisms (mainly large benthic foraminifera) and nutrient-dependent heterotrophic organisms (mainly rudists), with a remarkable rare occurrence of corals. Nutrients supplied from the emergent mainland probably promoted the development of heterozoan organisms. The vertical evolution of the ramp shows: a basal transgressive stage with facies retrogradation; a maximum flooding stage, and a regressive stage with aggradation and progradation of a distally steepened ramp. The presence and distribution of siliciclastics are problematic, since sands coming into the basin are likely to be rapidly and widely redistributed along the basin, taking into account the common storm, wave, and tidal processes preserved by the sedimentary facies. The presence of a clockwise NW-flowing longshore current is postulated to account for this distribution, which was likely induced by both dominant external currents around Iberia and wind-driven currents. These clockwise gyres facilitated the invertebrate dispersion into this enclosed basin and the local presence of upwelling. This could have been another source of episodic nutrient-rich waters from the deep ramp, which may have favored heterozoan development even in the more proximal and relatively shallower-water facies.

Keywords Homoclinal ramp · Benthic foraminifera · Rudists · Longshore currents · Coniacian · Iberian basin

Introduction

Cretaceous carbonate sedimentary environments developed during a period of high sea level, when extensive, intracontinental emergent areas, of probable low relief, were inundated by shallow seas. The facies architecture of these environments differs from modern environments due to the predominance of rudists and benthic foraminifera associations. Similarly, these shallow intracontinental seas exhibited low topographic gradients, resulting in a platform profile that differs from that of typical Quaternary platforms (Schlager 2005). Another remarkable feature of many Late Cretaceous basins in the Tethys realm is the coexistence of shoreline siliciclastic sands and platform carbonates (Bachman and Kuss 1998; Floquet 1998; Sanders and Pons 1999; El-Azabi and El-Araby 2007; Niebuhr et al. 2011; Andrieu et al. 2021).

The Coniacian carbonate sediments in the Iberian basin provide an excellent example of these differences in facies architecture. These carbonates were associated with one of the maximum peaks of sea level during the Late Cretaceous. They originated from the drowning of shallow intracontinental areas, which improved sediment preservation and led to a relatively complete sedimentary record of the carbonate

✉ J. F. García-Hidalgo
jose.garciahidalgo@uah.es

J. Gil-Gil
javier.gil@uah.es

A. Bretones
antonio.bretones@edu.uah.es

C. Boix
carme.boix@uah.es

[1] Departamento de Geología, Geografía y Medio Ambiente, Universidad de Alcalá, 28871 Alcalá de Henares, Spain

Published online: 30 March 2024

environments that developed in the basin. However, the detailed facies types and their distribution in the Coniacian deposits of the Iberian basin are not well understood. Few previous studies have focused on general aspects of the stratigraphic units and their cyclical organization within the Late Cretaceous framework of the basin (Floquet 1998; Segura et al. 2002; García et al. 2004; Martín-Chivelet et al. 2019), as well as their general palaeontological content (García-Hidalgo et al. 2012; Callapez et al. 2015). A comprehensive study of the facies, facies associations, architecture, and evolution of sedimentary environments within this basin has not yet been conducted.

Regarding the coexistence of shoreline siliciclastic and platform carbonates, these sedimentary systems comprise an inner platform siliciclastic facies belt, composed mainly of sands and sandstones (with minor conglomerates), and a range of different marine carbonate facies belts. The supply of siliciclastics to a basin is usually considered an inhibitor of carbonate development. However, for single stratigraphic intervals, they may coexist either as 1) "reciprocal sedimentation," when siliciclastic and carbonate components extend throughout the basin as separate facies of pure end-member systems according to sea-level cycles, leading to a separation into highstand carbonates and lowstand siliciclastics (e.g., Schlager 1991; Southgate et al. 1993; Tucker 2003; Campbell 2005; Gil et al. 2006; Tänavsuu-Milkeviciene et al. 2009; Schwartz et al. 2016; Val et al. 2019). 2) "Facies mixing" when the interplay between terrigenous input and carbonate production produces "mixed systems," where carbonate and siliciclastic grains are truly mixed in the same beds. The former is usually the preferred model for many Cretaceous sequences in the Iberian basin (e.g., Segura et al. 2002; García et al. 2004; Gil et al. 2010). Both groups of lithofacies belts have been widely studied from a sedimentological point of view, including local palaeogeographic distribution and facies patterns (e.g., Sanders and Pons 1999; El-Azabi and El-Araby 2007; Powell and Moh'd 2011; Andrieu et al. 2021). Jurassic and Cretaceous palaeogeographic maps (as well as other ages), from Europe to the Himalayas (e.g., Bachman and Kuss 1998; Zhang et al. 2004; Niebuhr et al. 2011; Andrieu et al. 2016), usually show these as distinct facies belts. One point that, however, has received very scarce research attention, namely why siliciclastics sourced to Cretaceous shorelines, were not then redistributed across the marine shelf areas, when energetic processes were pervasive (e.g., Powell and Moh'd 2011; Andrieu et al. 2021), and siliciclastic facies progradation is regarded as a common process. Therefore, it is challenging to understand why these siliciclastic and carbonate facies do not show truly mixed facies under those circumstances.

The Coniacian successions in the Iberian basin also offer a favorable opportunity to analyze and discuss all the factors that control the vertical and lateral variations of facies in different environments. This study can also help in reconstructing the depositional environments of the carbonate platform, basin palaeogeography, and palaeoceanography, which share many points in common with other Jurassic and Cretaceous basins of the Tethyan realm. The study also analyzes the different facies that make up the shorelines of the emergent Iberian massif, especially describing and interpreting the relationships between carbonate and siliciclastic sediments in a carbonate dominant environment.

The aims of this study are as follows: (1) to analyze the depositional facies and sedimentary environments of the Coniacian succession using macro- and microfacies data; (2) to propose a depositional model based on sedimentological and stratigraphic relationships, identifying the basic building blocks of the succession, and analyzing their vertical and lateral variations; (3) to determine the distribution of the different groups of organisms through the studied sediments and their relationships with sedimentary facies; (4) to analyze and compare the distribution of siliciclastic sediments between different sedimentary environments, and to address the problem of mixing siliciclastic–carbonate facies, and (5) to reconstruct the major palaeogeographic and palaeoceanographic controls on the evolution of this carbonate-siliciclastic ramp.

Geological setting

The Iberian basin was part of several shallow-marine basins surrounding the Atlantic and Tethyan realms during the Late Cretaceous. It was located south of the Eurasian plate, separated from it by the Basque and Pyrenean troughs (Fig. 1). At these times, this NW–SE-trending basin was bounded to the west and east by the emergent Iberian and Ebro massifs, respectively. Littoral terrigenous shoreline deposits occur on the Iberian margin of the basin. The "cul-de-sac" southern end of the basin includes marly littoral deposits commonly affected by pedogenic processes, but lacks connection with the Tethys further south (Fig. 1).

Within the studied area (Fig. 2), the Coniacian sediments contain a shallow-water carbonate succession of the Hortezuelos Formation (Fig. 3a) (Floquet et al. 1982). Toward the north, the Hortezuelos Formation grades laterally into the Nidáguila Formation (up to 155 m thick of fossiliferous marlstones and clayey limestones) and the lowermost part of the Nocedo de Burgos Formation at the top (limestones and clayey limestones) (Fig. 3a). To the south, the Hortezuelos Formation grades into the Alarcón Formation (Fig. 3a), which is composed of thin-bedded dolomitic limestones and organic-rich green marlstones (Gil et al. 2004).

The Coniacian age of the studied successions is well established due to the presence of the inoceramid *Platyceramus undulatoplicatus*, primary marker of the Santonian

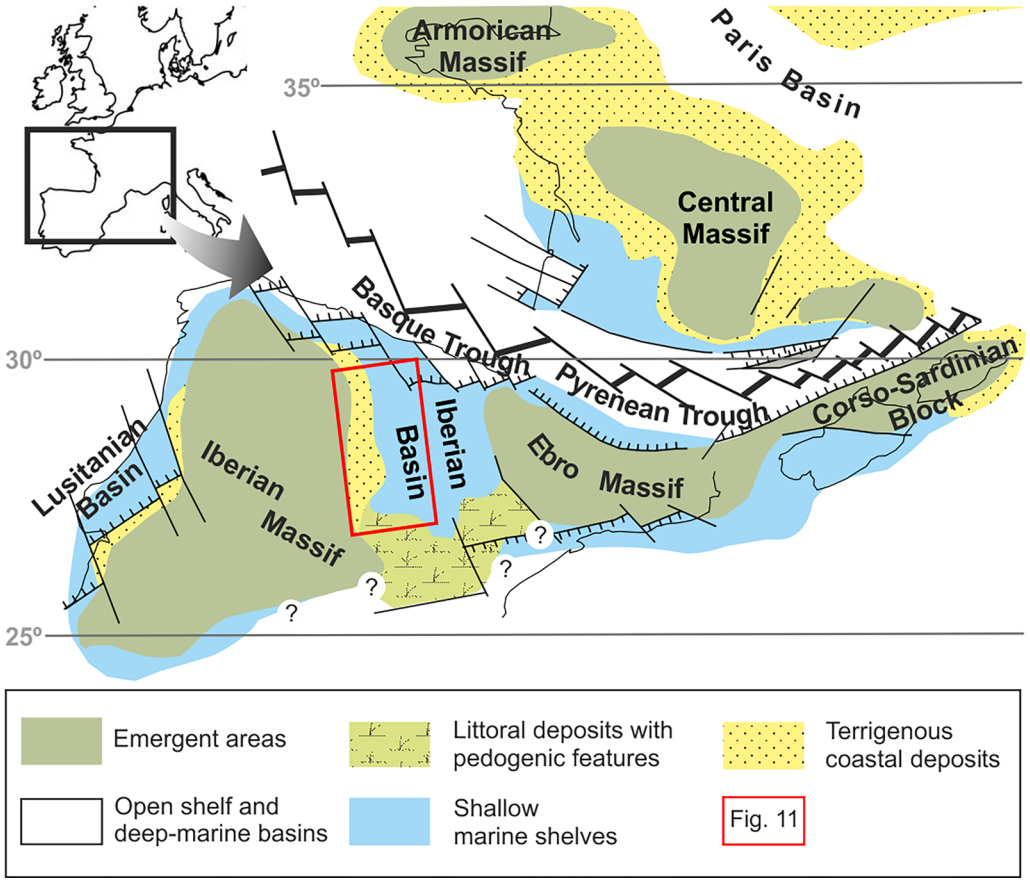

Fig. 1 Palaeogeographical scheme of the Iberian basin during Coniacian times, showing the main depositional environments and its location within the Tethyan Realm. Based on Floquet and Hennuy (2001) and modified from García-Hidalgo et al. (2012). Red rectangle shows location of Fig. 11

stage (Lamolda and Hancock 1996), in the basal beds of the overlying sediments (Nocedo de Burgos Fm) at the Villamartín Sect. (1 in Fig. 3a; Gallemí et al. 2007). Coniacian ammonites have also been commonly found. *M. ewaldi, T. hispanicus, G.margae* and *P. iberiense*, subzones characterize the Middle Coniacian (Fig. 3a). *P. burgueoisi* and *Hemitissotia spp.* subzones correspond to the Late Coniacian (Fig. 3a; García-Hidalgo et al. 2012). On the other hand, Coniacian rudist faunas (Gil et al. 2002, 2009, 2024) have been widely described within the *Hemitissotia spp.* subzone.

In terms of sequence stratigraphy (as defined by Catuneanu et al. 2011), the studied sediments represent a single depositional sequence (DS-2 sensu García-Hidalgo et al. 2012), bounded by two major sequence boundaries (SB). SB recognition is based on the presence of major sedimentary discontinuities, diagenetic overprints, and breaks in the vertical succession of facies, reflecting major changes in sedimentary trends (Floquet 1998; García-Hidalgo et al. 2012). The lower SB represents a major surface of basal onlap on the underlying sequence. The upper SB occurs within a gradational interval of facies change (conformable horizon), representing an important advance of the shallower facies basinward (a maximum regressive surface sensu Catuneanu et al. 2011). DS2 maximum flooding (mfs) is located at the base of the *Hemitissotia spp*. subzone. The mfs is underlain by a retrogradational pattern with a deepening-upward trend, and it is overlain by a progradational pattern with a shallowing-upward trend (García-Hidalgo et al. 2012; Fig. 3b). The presence of abundant cephalopods, with smooth and compressed oxycones (*H. ceadouroensis/celtiberica-turzoi*) representing well-adapted active swimmers, is related to the deeper facies of DS2, corresponding to the mfs (Segura et al. 2014). DS2 within these boundaries is composed of a transgressive and a highstand normal regressive systems tracts (TST and HNR, Fig. 3a).

Materials and methods

Twenty-six complete stratigraphic sections were measured in the studied area (Fig. 2) to create three cross-sections: an NW–SE longitudinal cross-section (Fig. 3) and two, transverse NE–SW cross-sections (Figs. 4 and 5). The

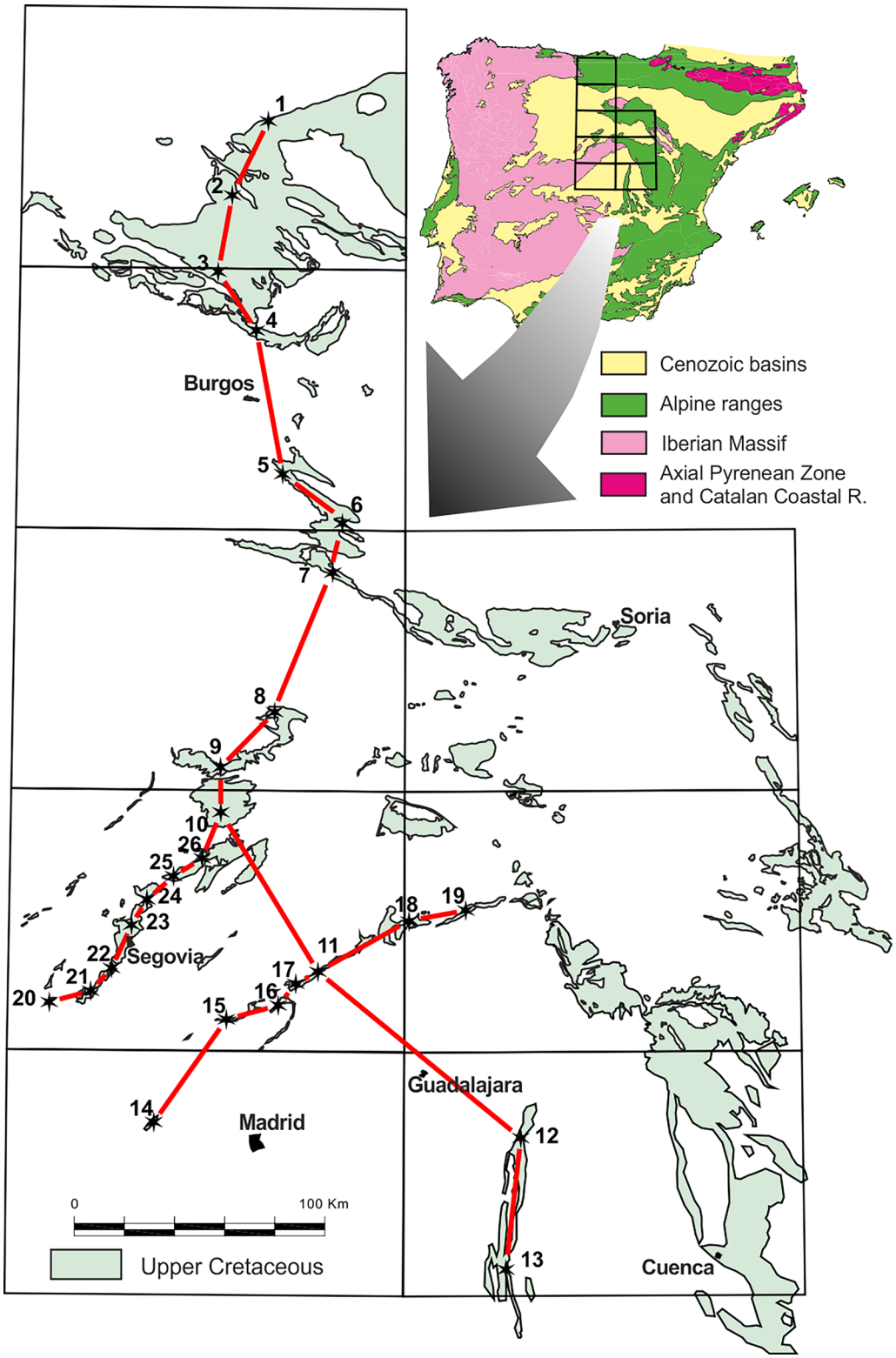

Fig. 2 Geographical scheme of the study area, showing the upper Cretaceous outcrops in the central part of the Iberian Peninsula, sheets of the 1:200,000 Spanish Geological Map (gridding), the cross-sections (red lines) of Figs. 3, 4 and 5, and the following stratigraphic key sections: **1** Villamartín de Sotoscueva; **2** Turzo; **3** Nidáguila; **4** Ubierna–Peñahorada; **5** Cuevas de San Clemente; **6** Contreras–Hoz de Silos; **7** Doña Santos; **8** El Casuar; **9** Castroserracín–Castrojimeno; **10** Sepúlveda; **11** Barranco de las Cuevas; **12** Embalse de Entrepeñas; **13** Estrecho de Paredes; **14** Valdemorillo; **15** Soto del Real; **16** Embalse de Pedrezuela; **17** Torrelaguna; **18** Muriel; **19** Alcorlo; **20** Ituero y Lama; **21** Valdeprados; **22** Hontoria; **23** La Lastrilla; **24** La Higuera; **25** Caballar; **26** Pajares de Pedraza

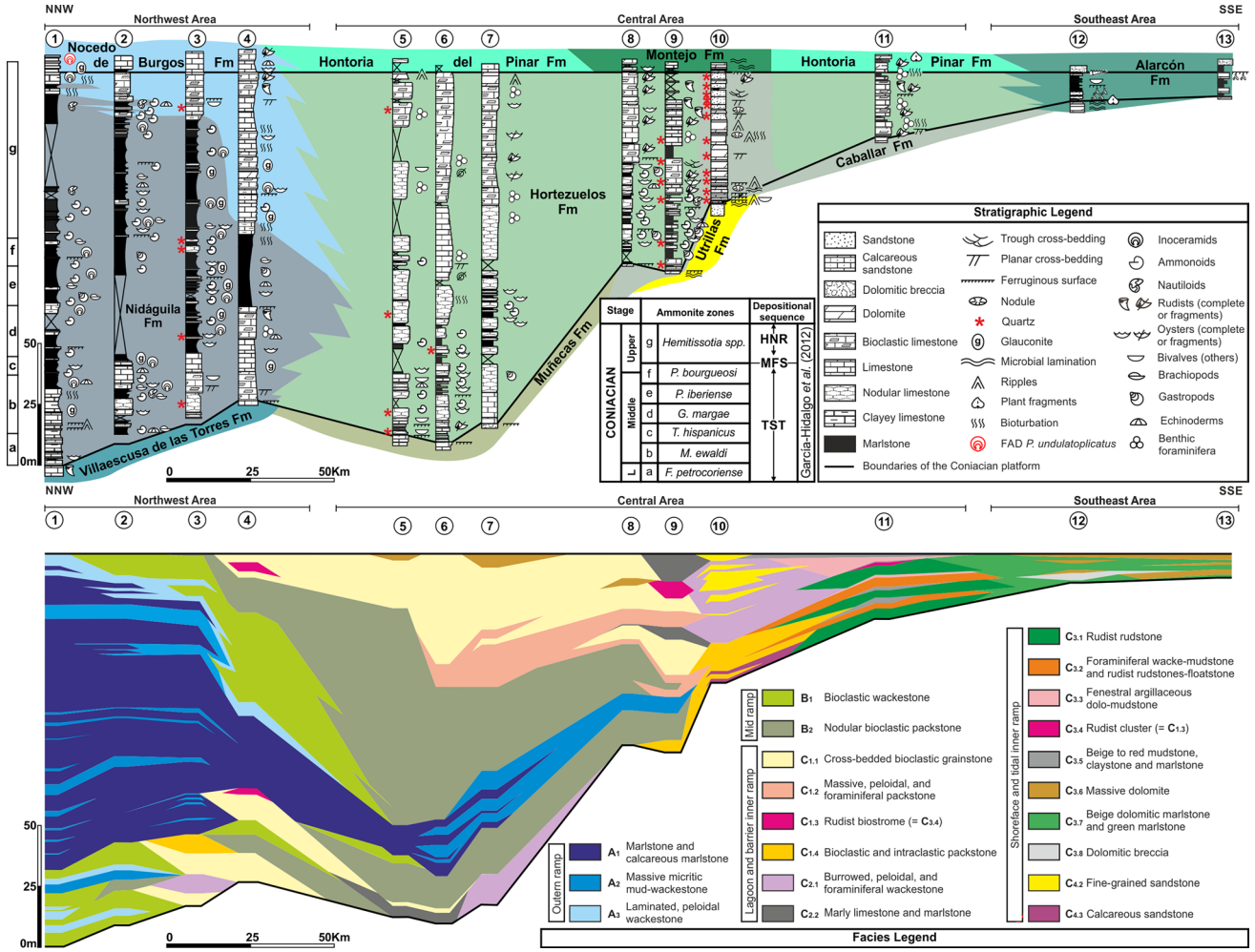

Fig. 3 NW–SE cross-section of the Coniacian platform within the Iberian Basin, showing the stratigraphic successions, the chronostratigraphic framework, and the lithostratigraphic units in each reference area (**a**) and the facies distributions (**b**). See Fig. 2 for location and name of key sections

longitudinal cross-section shows a wedge-shaped, thinning southward, geometry with a thickness of 161 m in the north, reaching about 12 m at the southeastern end (Fig. 3). Both transverse cross-sections show also a wedge-shaped geometry, thinning southwestwards against the emergent Iberian massif.

The studied sections were measured, sampled, and described bed-by-bed using rock color, stratification patterns, and sedimentary structures and textures. More than 100 rock samples were collected and examined in 25 standard thin-sections under a microscope to determine the selected lithofacies. The sandstone lithofacies were described following the classification of Pettijohn et al. (1987). Description of carbonate microfacies includes grain size, composition, depositional texture, and fossil content (Flügel and Munnecke 2010). The classification of Dunham (1962) as expanded by Embry and Klovan (1971) is used for carbonates. Microfacies are named following the order of relative amounts of grain types; aggregate grains are described as intraclasts. A size limit of 0.2 mm is used to distinguish between "mud peloids" (or "lithic peloids") and intraclasts (Flügel and Munnecke 2010).

Results

Facies association and palaeoenvironmental interpretation

Based on lithology, sedimentary structures, and biogenic and fossil content (macro- and micro-fauna), 23 facies are identified (Table 1). The carbonate succession is interpreted as being deposited on an open homoclinal ramp (Read 1985), with three main depositional environments (Burchette and Wright 1992): outer ramp (facies association A), mid ramp (facies association B), and inner ramp (facies association

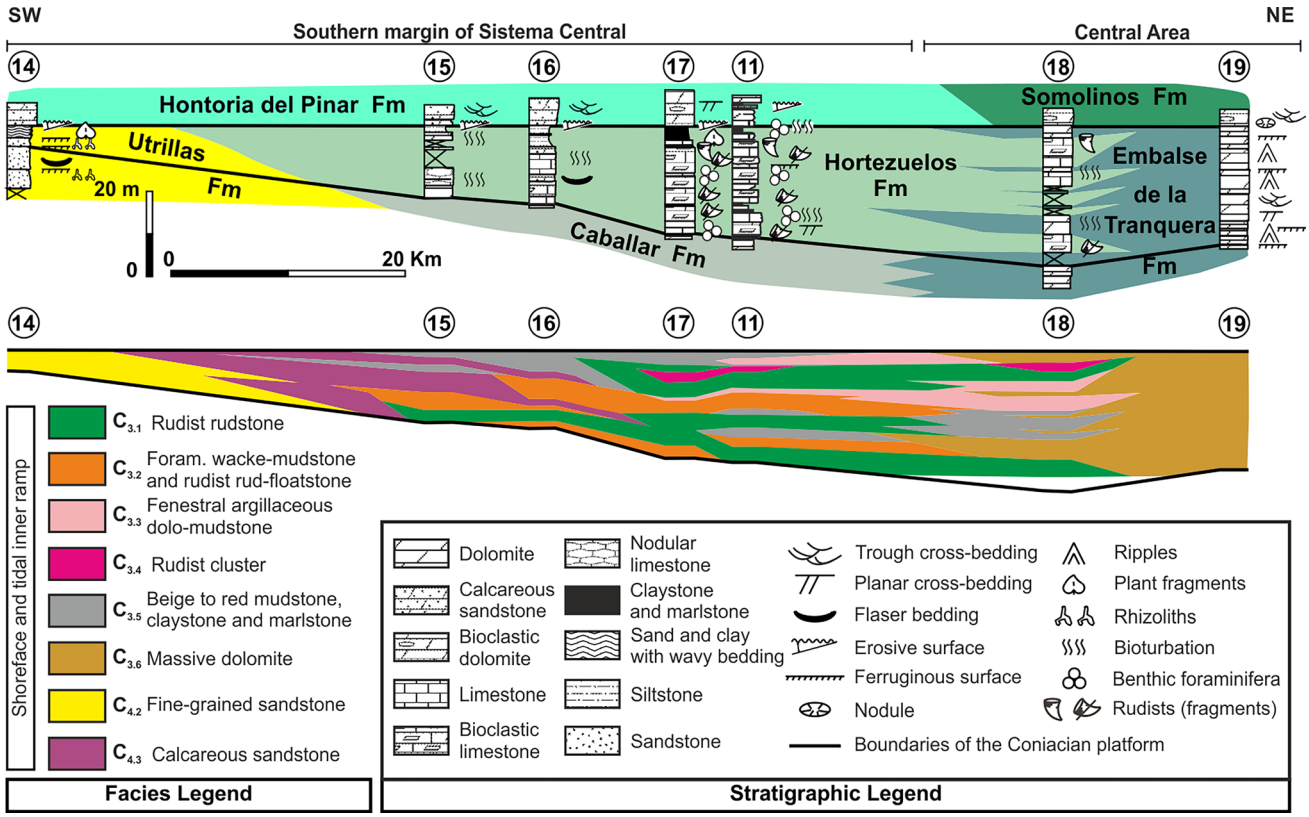

Fig. 4 SW–NE transverse section of the Coniacian platform along the southern margin of the Sistema Central (SW margin of the Iberian basin), showing the stratigraphic successions and lithostratigraphic units in each reference area (**a**) and the facies distributions (**b**). See Fig. 2 for location and name of key sections

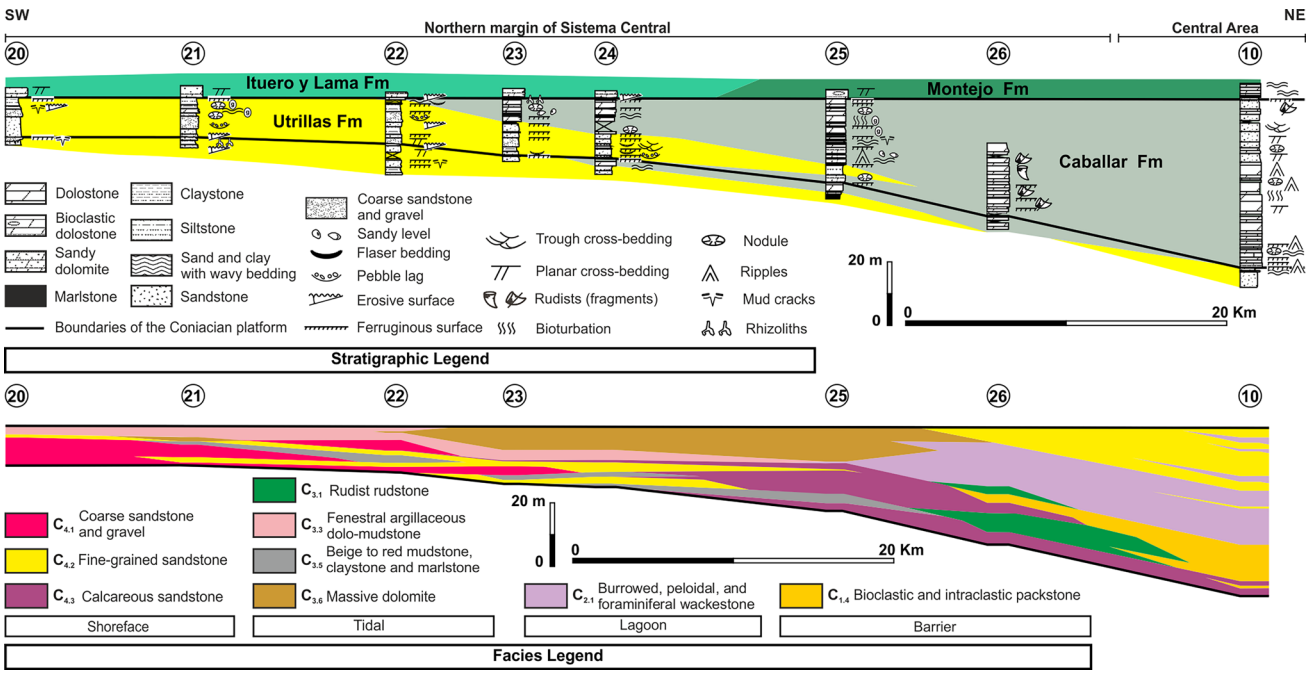

Fig. 5 SW–NE transverse section of the Coniacian platform along the northern margin of the Sistema Central (SW margin of the Iberian basin), showing the stratigraphic successions and lithostratigraphic units in each reference area (**a**) and the facies distributions (**b**). See Fig. 2 for location and name of key sections

Table 1 Description of facies, including fossils and biogenic structures, with suggested processes and features of depositional environments

Facies		Description	Fossils and biogenic structures	Depositional environments
A	A1, Marlstone and calcareous marlstone	Massive, dark gray, organic matter-rich marlstone	Oxyconic ammonoids, nautiloids, inoceramids, bivalves (mainly gryphaeas), gastropods (including turritellids), echinoderms and bryozoans. Rare *Thalassinoides*	Low-energy, quiet, depositional setting well below storm wave base; local anoxic seafloors Outer ramp
	A2, Massive, mudstone and wackestone	Massive, thin-bedded, gray limestone (mudstone to wackestone texture) with an abundant micritic matrix finely recrystallized; Glauconite	Echinoids, ostracods, *Gryphaea,* bivalves (including inoceramids, some bioeroded and colonized by annelids), gastropods, bryozoans, ammonoids, and nautiloids. Planktic foraminifera and rare presence of small benthic foraminifera (probably resedimented). *Thalassinoides*	Low-energy, quiet, depositional environment below storm wave-base; oxic bottoms. Development of local firmgrounds with bioerosion of some of the skeletal grains Outer ramp
	A3, Laminated, peloidal wackestone	Laminated limestone with a wackestone and localized packstone texture. Micritic matrix locally recrystallized. Micritic peloids (possible fecal origin)	Bivalves (including oysters), gastropods, ammonoids, echinoderms, bryozoans, ostracods, and planktic foraminifera; very rare presence of green algae (including dasycladacean) and small benthic foraminifera	Low-energy, quiet, depositional setting below storm wave-base; oxic bottoms. Well agitated, stenohaline waters in an open marine environment Outer ramp
B	B1, Bioclastic wackestone	Gray, thin-bedded limestone (mostly wackestone, with common patches of mudstone and minor packstone texture). Dark glauconite grains; red ferroan mottling	Bivalves (including pycnodont oysters), gastropods, echinoids, ostracods, bryozoans, serpulids; Abundant planktic foraminifera, and common presence of small benthic foraminifera (textulariids, miliolids unidentified rotaliids, discorbidae); possible *Lenticulina*	Low- to moderate-energy setting above storm wave base and below fair-weather wave base; the abundance of marine fauna requires the persistence of well-agitated, stenohaline waters in an open marine environment Mid ramp
	B2, Nodular, bioclastic packstone	Grayish limestone with characteristic nodular bedding and a packstone texture (localized wackestone). Presence of glauconite and poor sorted phosphatic grains, and fine-grained, angular to subangular quartz grains. Presence of ferruginized and bioperforated oysters; locally rounded intraclasts are also common	Ammonoids, bivalves, echinoderms, bryozoans, ostracods, gastropods, serpulids, and rare green algae; planktic and common benthic foraminifera, the latter represented by small forms (textulariids, discorbidae, miliolids, rotaliids) and larger benthic foraminifera (*Minouxia*, *Lenticulina*?, *Nummofallotia cretacea*, *Pararotalia* spp., and *Rotorbinella* sp.). *Thalassinoides* burrow systems	Moderate-energy setting above storm wave base and below fair-weather wave base. Nodular bedding commonly associated with bioturbation by *Thalassinoides* burrow systems (firmgrounds), enhanced by postsedimentary compaction and diagenesis Mid ramp
	B3, Marlstone with oyster boundstone	Massive marlstone with interbedded oyster *Pycnodonte* boundstone	Ammonoids, bivalves (including *Pycnodonte*) gastropods, encrusting bryozoans, and serpulids	Low-energy setting below fair-weather wave base, low rates of sedimentation. Autochthonous concentrations of mostly articulated oyster shell clusters, dominated by *Pycnodonte* shells in a marly, soft-ground, environment Mid ramp

Table 1 (continued)

Facies		Description	Fossils and biogenic structures	Depositional environments
C				
C1	C1.1, Cross-bedded bioclastic grainstone	Cross-bedded (large-scale planar and trough cross-bedding) or massive, moderate to well-sorted, bioclastic limestone in tabular beds with scoured or slightly erosive bases and flat tops. Grainstone and locally packstone with a scarce presence of recrystallized micritic matrix. Well-rounded intraclasts, abundant coated grains (most of them with dissolved nuclei or micritized skeletal grains), minor ooids, and scarce quartz extraclasts	Bivalves, gastropods, solitary and scleractinian corals, chaetetid sponges, brachiopods, echinoids, bryozoans, calcareous dasycladacean algae (*Acicularia*?), ostracods small and large benthic foraminifera are common; the latter include *Pseudonummoloculina, Pseudocyclammina, Dicyclina, Cuneolina, Dictyopsella, Nezzazatinella, Vidalina*, possible *Cyclolina, Minouxia,* textulariids, miliolids, discorbidae, and unidentified rotaliids. Minor presence of serpulids and rudists, and rare red algae fragments	High-energy shallow setting above fair-weather wave base and close to the low tide level, constant wave agitation High-energy inner ramp
	C1.2, Massive, peloidal, and foraminiferal packstone	Thin- to thick-bedded, massive tabular beds of peloidal and foraminiferal-rich packstone, with non-erosive, planar bases and tops. The packstone is characterized by fine-grained, subrounded, micritic peloids, and benthic foraminifera and fragmented, moderately abraded, and slightly packed debris of bivalves and echinoderms embedded in a lime mud matrix	Abundant gastropods, echinoids, bryozoans, dasycladacean algae, bivalves, and common presence of small and large benthic foraminifera. Small forms (textulariids, discorbidae, miliolids, rotaliids) and larger benthic foraminifera: *Rotorbinella* sp., *Pararotalia* spp., *Nummofallotia cretacea*, *Pseudocyclammina* aff. *sphaeroidea* (?), *Nonion senonicus*, *Pseudonummoloculina*?	Moderate-energy, shallow setting within the euphotic zone, reflecting oligotrophic conditions. Most of the peloids having elongated shapes most likely represent fecal pellets Moderate-energy inner ramp
	C1.3, Rudist biostrome (Boundstone)	Open-to-close cluster reefs within autochthonous and parautochthonous fabrics, developed above reworked bioclastic beds (segment reefs), grading upwards to oligospecific or monospecific, closely packed, autochthonous frame reefs. The matrix represented by skeletal wackestone to packstone with a large proportion derived from bioerosion and mechanical breakdown of rudist shells; absence of benthic foraminifera	Rudists are widely predominant in these limestones, with subordinate gastropods and echinoids. Rudists are characterized by species belonging to the Radiolitids, biradiolitids, and hippuritids genera	High hydrodynamic gradient setting, with decreased sedimentation rates and high biological competition for the (limited) available space and shallowing-upwards trends, even with subaerial exposure events Shallow, inner ramp (subtidal)

Table 1 (continued)

Facies		Description	Fossils and biogenic structures	Depositional environments
	C1.4, Bioclastic and intraclastic packstone	Massive, moderate to well-sorted limestone in decimeter-scale tabular beds with scoured bases and flat tops, and a bioclastic and intraclastic packstone with local rudstone and floatstone texture. Skeletal grains comprise rudist and oyster bioclasts, and rare small solitary coral fragments and echinoid debris. Rudist bioclasts (radiolitids and hippuritids) comprise mainly isolated and oriented lower valves. Medium-grained, subrounded, micritic-rich intraclasts are present	Rudist, oysters (*Pycnodonte*) and echinoid debris; minor benthic foraminifera (*Cuneolina, Dicyclina, Minouxia*?, small miliolids, textulariids, discorbidae); and rare ostracods	Agitated, shallow-water, above fair-weather wave base. Reworked skeletal fragments derive from the erosion of boundstones in nearby environments during storm events. Rudists clusters are rarely preserved Inner ramp area
C2	C2.1, Burrowed, peloidal, and foraminiferal wackestone	Well-bedded, planar, tabular limestone with flat and sharp bases and tops, and with an overall wackestone texture. Common presence of subrounded, fine to medium-grained micritic peloids and coated grains	Abundant small and large benthic foraminifera, gastropods, bryozoans, bivalves (including rudists), dasycladacean green algae (including *Acicularia*?), echinoids, and ostracods. Scarce red algae and coral fragments. Burrowing is locally common	Low-energy sedimentation in a very shallow-marine back-barrier setting, at the upper part of the euphotic zone, with relatively low-energy currents Protected inner ramp (lagoon)
	C2.2, Marly limestone and marlstone	Massive marly limestone and marlstone, including thin beds of limestone (floatstone) with a nodular aspect; silt and clayey layers are present	Bivalves, gastropods, small benthic foraminifera; local chaetetids, echinoderms, and corals; and rare plant fragments and carbonaceous remains. Bioturbation is common to rare. Presence of rudists as thin, open to close pauciespecific cluster reefs (framestone) or as isolated specimens (radiolitids and hippuritids). Shells in life position, most of them with both well-preserved valves. Elevator (vaccinitids), reclining (praeradiolitids), or forward-leaning forms embedded in marly or mudstone, soft matrix	Low- to moderate-energy setting within a subtidal area in a back-barrier environment. The reclining or forward-leaning rudists indicates a need to adjust to the constant influx of fine-grained material. Segments reefs composed of disarticulated shells are probably related to storm events that remobilized soft-ground seafloors. The presence of corals and chaetetids suggests an environment in the photic zone Shallow, protected, inner ramp (lagoon)
C3	C3.1, Rudist rudstone	Dark-gray, medium to thick-bedded, rudist-rich rudstone (rarely floatstone) with a grainstone texture matrix. The rudist debris are very poor to well-sorted, with locally oriented shells. Subrounded, micritic-rich intraclasts are present	Rudist fragments, small benthic foraminifera (miliolids, textulariids, and discorbidae), and large benthic foraminifera forms (*Cuneolina, Dicyclina*, and possible *Minouxia*)	Relatively high-energy setting, sedimentation of the bioclastic fraction derived from the reworking of rudist clusters Carbonate tidal flat (open, shallow subtidal)

Table 1 (continued)

Facies	Description	Fossils and biogenic structures	Depositional environments
C3.2, Foraminiferal wackestone-mudstone and rudist rudstone-floatstone	Massive, thin- to thick-bedded, foraminifera-rich wackestone and mudstone with rudist debris. Most rudists are either loosely packed, isolated shells (rudstone), or small broken clusters showing an open, parautochthonous rudist fabric within a bioturbated bioclastic matrix (floatstone). Bioturbation is common	Rudists and other bivalves, small and large benthic foraminifera, echinoids, calcareous red and green algae, and gastropods. *Thalassinoides* and other irregular burrows	Low- to high-energy setting as suggested by the presence both of a muddy matrix and rudist rudstones and other bioclasts made up of partially eroded and broken, and foraminiferal shells resulting from weak and rare storm and wave processes. Interpreted as accumulated in a shallow environment Carbonate tidal flats (open, shallow subtidal)
C3.3, Fenestral, dolo-mudstone	Whitish, thin-bedded, parallel-laminated, and fenestral limestone (mudstone and locally wackestone) and dolomite with flat bases and hardened, highly irregular (bioeroded) or flat, erosive (bioperforated) tops. Irregular fenestral laminations of mm-scale alternation of micritic laminae and horizontally elongated fenestrae porosity occluded by fine to medium-crystalline calcite and dolomite cements. Some laminae have a dense clotted-peloidal microfabrics	Rare presence of small benthic foraminifera (miliolids, textulariids, discorbidae, ataxophragminids, possible nezzazatinellids), ostracods, and fragments of thin-shelled bivalves, echinoids, and gastropods. Small irregular burrows	Low-energy setting, development of microbial mats (stromatolites) Carbonate tidal flats (intertidal-subtidal)
C3.4, Rudist cluster	Medium- to thin-bedded micritic limestone with rudists in life position, forming small clusters of several individuals or"thickets " of loose specimens partially buried in a fine micritic mud, which fills the internal cavities; the micritic matrix is locally replaced by very fine crystalline dolomite	Rudists (mainly radiolitids)	Low-to-moderate-energy setting, rudists growing on a muddy seafloor Carbonate tidal flats (subtidal)
C3.5, Beige to red mudstone, claystone, and marlstone	Very thin-bedded beds and joints of beige to red mudstone, claystone, and platy marlstone	Rare plant fragments and other carbonaceous remains	Low-energy setting, dominated by decantation processes. Low sedimentation rates and scarce input of plant remains from nearby emergent areas; iron accumulation (reddening) suggesting the development of sedimentary breaks under oxidizing conditions Carbonate tidal flat (intertidal-to-supratidal)
C3.6, Massive dolomite	Beige, thin- to medium-bedded, massive dolomite with large nodules. The original rock has been pervasively replaced by abundant, fine to medium-crystalline dolomite/calcite	Rare, plant remains as small, black fragments	Low-energy setting dominated by carbonate precipitation, scarce inputs of plant remains from nearby emergent areas Carbonate tidal flats (mainly intertidal)

Table 1 (continued)

Facies		Description	Fossils and biogenic structures	Depositional environments
	C3.7, Beige dolomitic marlstone and green marlstone	Beige or green marlstone with massive or platy texture	No fossils identified	Low-energy setting, dominated by decantation processes. Alternation of reducing and oxidizing environment, controlled by flooding onto extensive mudflats with a strong continental influence Carbonate tidal flats (intertidal-to-supratidal)
	C3.8, Dolomitic breccia	Nodular, laminar and massive, yellow and brown, brecciated dolomite with vertical, open joints; some nodules resemble chicken-wire structures; minor terrigenous clay and silt	No fossils have been identified; possible root molds	Low-energy setting. Palaeosol dolocretes originated by in situ brecciation and caused by prolonged subaerial exposure or the penetrative growth of roots Carbonate tidal flats (supratidal)
C4	C4.1, Coarse sandstone and gravel	Planar-laminated and cross-bedded, coarse- to medium-grained sandstone and well-sorted gravel with planar and slightly scoured, erosive bases. Local gravel lags	Local plant remains and root traces	Medium-to-high energy in a coastal siliciclastic setting. Plane bed sediment transport related to wave action. Bedload sedimentation from unidirectional flows as indicated by the presence of cross-bedding due to the migration of sandy asymmetric dunes. Low-regime tractive processes; dune migration by waves, probably limited tidal range, and abundant sand supply Upper shoreface—Foreshore
	C4.2, Fine-grained sandstone	Thin-bedded, massive or parallel- to cross-laminated sandstone and silty sandstone with sharp basal and top contacts. Cross-bedding sometimes with herringbone appearance, with cross-sets from 10 to 30 cm in thickness and from 20 to 30º in foresets dip. Wave ripples also occur at the top of some cross-strata. The sandstone is micaceous rich, with fine to medium sand-sized monocrystalline quartz grains	Rare fragments of thin-shelled rudists. Rare presence of burrowing	Low-to-high energy in a coastal siliciclastic setting. Quick sand accumulation from suspension; abundant sand supply. Accumulation of small to medium-sized dunes and bars. Continuous reworking and movement of sand by variable bidirectional flow regime. Herringbone indicate bidirectionality in flow directions. Rudists' fragments transported from nearby carbonate lagoon areas. Biogenic structures also suggest sediment burrowing during periods of low-energy Shoreface
	C4.3, Calcareous sandstone (quartz-rich packstone)	Fine-grained, bioclastic-rich calcareous sandstone (packstone), with common micritic matrix and very abundant, very fine-grained, subangular quartz grains. Minor presence of fine to medium-grained, subrounded peloids and very rare, very fine-grained phosphatic grains (glauconite?)	Abundant echinoids and bivalves. Common ostracods and bryozoans, and minor presence of small benthic foraminifera and planktic foraminifera	Mixed facies originated by the reworking of carbonate grains in relation to the coastal siliciclastics and inner ramp carbonates. Moderate and high energy setting close to fair-weather wave base Lower shoreface and/or inner ramp with a large siliciclastic influence

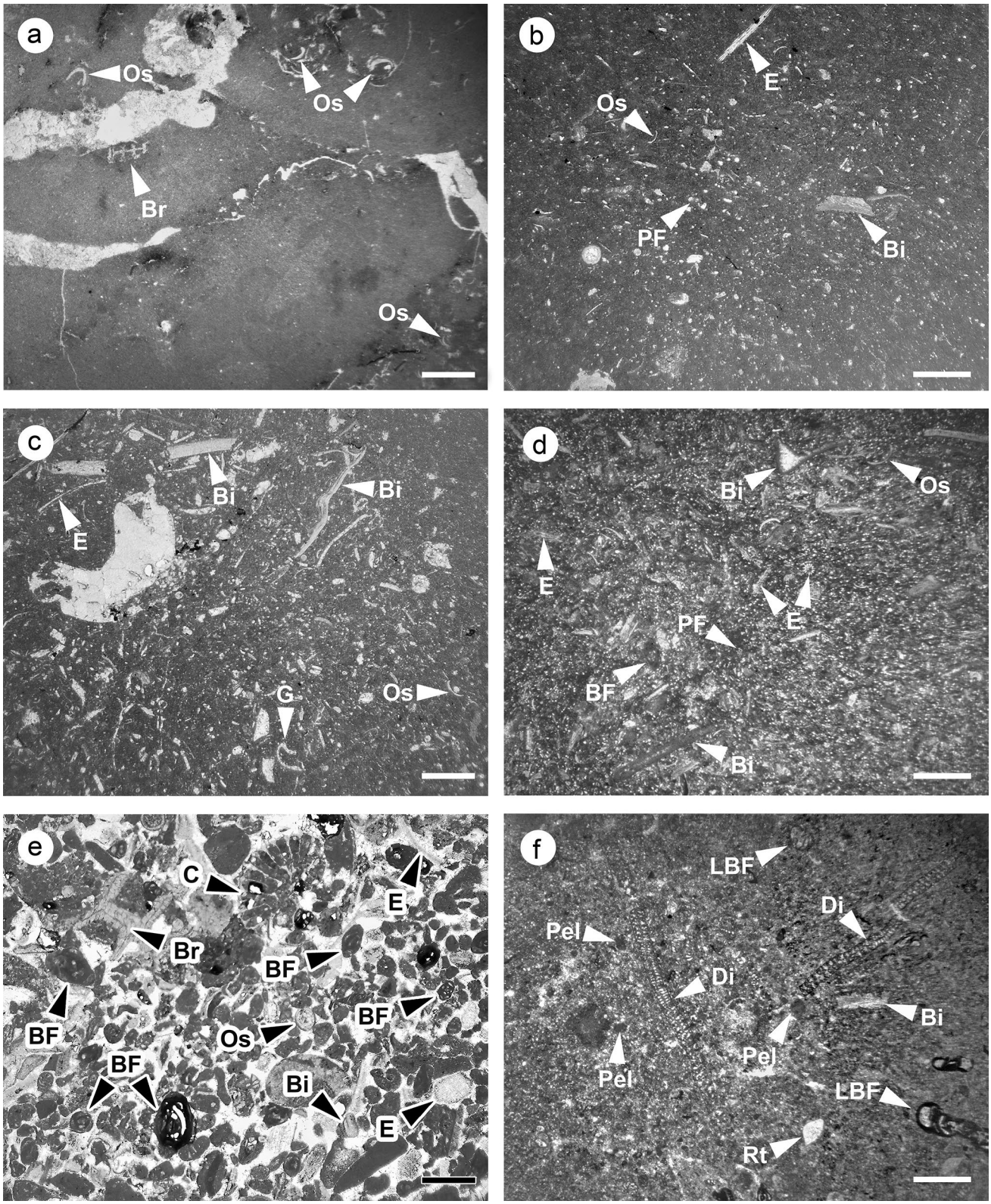

C). According to the ramp model and based on sedimentary features and/or components, the inner ramp is subdivided into: 1) high-energy shoals acting as low-relief barriers (facies C1); 2) a low-energy sheltered lagoon (facies C2); 3) carbonate tidal flats (facies C3), and 4) a siliciclastic, shoreface facies belt (facies C4). Facies codes, associations,

◂**Fig. 6** Photomicrographs of selected facies from outer (**A**), mid (**B**), and high-energy (C1) inner ramp settings. All scale bars represent 1mm. **a** Facies A2, *Massive mudstone and wackestone*. Mudstone with localized wackestone texture, with an abundant micritic matrix finely recrystallized and minor presence of ostracods (Os), bryozoan (Br), and echinoid fragments. Sample 22,030,105, Castroserracín section; **b** Facies A3, laminated, peloidal wackestone. Wackestone with locally recrystallized micritic matrix, and a skeletal assemblage comprising planktic foraminifera (PF), echinoid (E) and bivalve (Bi) fragments, ostracods (Os), and small benthic foraminifera. Sample 22,051,127, Contreras section; **c** Facies B1, Bioclastic wackestone. Wackestone with local packstone texture (possible bioturbation), with echinoid (E) and bivalve (Bi) fragments, ostracods (Os), and gastropods (G). Sample 22,051,125, Contreras section; **d** Facies B2, nodular bioclastic packstone. Packstone with fine-grained quartz and phosphatic grains. The skeletal grains comprise planktic foraminifera (PF), ostracods (Os), echinoderm (E), bivalve (Bi), and bryozoan fragments. Minor presence of small benthic foraminifera (BF). Sample 22,030,119, Castroserracín section; **e** Facies C1.1, Cross-bedded bioclastic grainstone. Grainstone with abundant skeletal grains, comprising small (BF) and large benthic foraminifera, bryozoan (Br), echinoid (E), bivalve (Bi), serpulids, ostracods (Os), and green algae fragments. Note the presence of a coral (C) fragment. Sample 22,051,108, Cuevas de San Clemente section; **f** Facies C1.2, Massive, peloidal and foraminiferal packstone. Packstone with locally recrystallized micritic matrix. Common presence of very fine micritic peloids (Pel). The skeletal assemblage is dominated by large benthic foraminifera [LBF; note the presence of *Dicyclina* (Di), rotaliids (Rt), and porcelaneous forms in the image]. Minor presence of ostracods and bivalve (Bi) fragments. Sample 22,030,124, Castrojimeno section. See Fig. 2 for location and name of key sections

descriptions, and environmental interpretations are summarized in Table 1. Microfacies types, microfossil content, and their corresponding field aspects are shown in Figs. 6, 7, 8, 9.

Outer ramp facies association (A)

Three facies characterize this association: A1, Marlstone and calcareous marlstone (Fig. 8a), A2, Massive mudstone and wackestone (Fig. 6a and 8b), and A3, Laminated, peloidal wackestone (Fig. 6b and 8b). The outer ramp facies are marked by the presence of abundant macrofauna (Table 1). Burrowing is rare, but large burrows (*Thalassinoides*) are locally present. Thin-sections of the outer ramp facies are characterized by the presence of planktic foraminifera, phosphatic grains, glauconite, and a lime mud matrix.

Usually, at outcrop, the outer ramp facies form characteristic facies sequences A1–A2–A3 that grade from marlstones to mudstones, and finally wackestones (Fig. 8c). From field views, facies A2 are easily recognizable by their poorly indurated, platy, homogeneous and weathered aspect, whereas facies A3 are more resistant (Fig. 8c).

The fine grain-size and absence of sedimentary structures suggest a low-energy, quiet, depositional environment below storm wave base. The rare, burrowed, calcareous beds with ferruginized surfaces can be interpreted as local condensed surfaces (Christ et al. 2012). Besides, the common presence of glauconite and phosphatic grains is also usually associated with stratigraphic condensation (Carson and Crowley 1993; Hillgärtner 1998), suggesting a longish residence time of the sediments on the seafloor. The abundance of planktic foraminifera, inoceramids, echinoids, and bryozoans, and the paucity of benthic foraminifera (which, when present, were probably remobilized from shallower environments), suggest deposition in an open, outer ramp setting. The presence of abundant nektonic ammonites supports this interpretation.

Mid-ramp facies association (B)

Three facies were identified: B1, Bioclastic wackestone (Fig. 6c), B2, Nodular bioclastic packstone (Fig. 6d), and B3, Marlstone with oyster boundstone. They are characterized by a mixture of planktic and benthic foraminifera, ammonites, bivalves (including pycnodonts), echinoderms and gastropods. Bioturbation is indicated by the presence of *Thalassinoides* burrows. The non-skeletal grains comprise glauconite, fine- to very coarse-grained phosphatic grains and very fine to fine-grained quartz grains, which are angular to subangular.

Bioclastic wackestone (B1) is commonly massive and thin-bedded with a matrix composed of carbonate mud (Fig. 6c), which is distinctive for low energy and low rates of sedimentation. The packstone texture (B2; Fig. 6d) and the poor sorting of skeletal components (bivalves, echinoderms, bryozoans) indicate a moderate-energy environment. The presence of nodular bedding is commonly associated with bioturbation by *Thalassinoides* burrow systems, enhanced by postsedimentary compaction and diagenesis (Mangano and Buatois 1991). *Thalassinoides* also suggests periods of low sediment input (Myrow 1995; Rodríguez-Tovar et al. 2008), excavated in a firmground (Glossifungites Ichnofacies; Seilacher 1967; MacEachern et al. 1992), where crustacean burrower activity was an important process.

Intercalated within facies B2 is the presence of nodular marlstones rich in fauna with thin oyster (*Pycnodonte*) layers in life position (B3 boundstone). The boundstones are dominated by *Pycnodonte (C.) costei* assemblages (Callapez et al. 2015) and consist of an autochthonous concentration of articulated individuals, with other attached oyster species. They appear in life positions as recliners adapted to soft-bottom mid-ramp environments (cup-shaped recliners of Seilacher 1984), and are found beneath fair-weather wave base, an environment that provided stable and oxygenated substrates adequate to establish an important colonization by infaunal bivalves and echinoids (Callapez et al. 2015).

Facies association B represents higher hydrodynamic gradients than facies association A (Fig. 8c). The abundance of echinoderms and bryozoan fragments, and the presence of planktic foraminifera require the persistence of open-marine

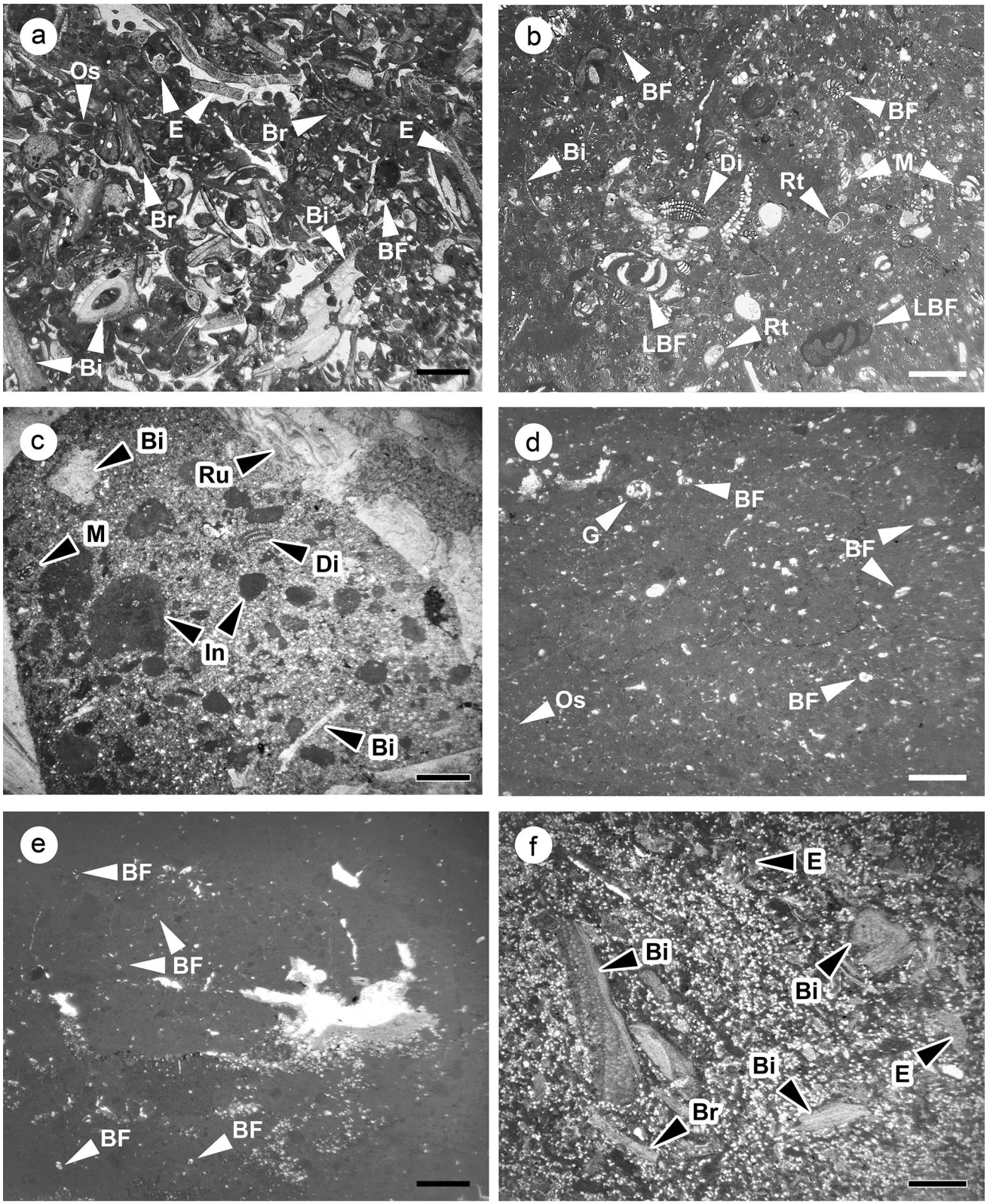

conditions in a mid-ramp setting under conditions of normal oxygenation and salinity. The environmental interpretation is also supported by the presence of rare ammonites. Morphologically, the ammonites are less hydrodynamic with moderately ornamented shells and evolute discocones and platycones. The scarce hydrodynamic efficiency is

◂**Fig. 7** Photomicrographs of selected facies from inner ramp settings. All scale bars represent 1mm. **a** Facies C1.4, Bioclastic and intraclastic packstone. Pack-grainstone with abundant skeletal grains including bryozoan (Br), bivalve (Bi), echinoid (E), gastropod and green algal fragments, ostracods (Os), and benthic foraminifera (BF). Sample 22,052,518, Nidáguila section; **b** Facies C2.1, burrowed, peloidal, and foraminiferal wackestone. Wacke–packstone with a locally recrystallized micritic matrix. The skeletal assemblage is dominated by small benthic foraminifera (BF; e.g., rotaliids (Rt) and miliolids (M)), large benthic foraminifera (LBF; e.g., *Cuneolina*, *Dicyclina* (Di), *Cyclolina*, *Dictyopsella*), and minor presence of bivalve (Bi) and echinoid fragments. Sample 22,052,515, Nidáguila section; **c** Facies C3.1, Rudist rudstone. Rudstone with a common recrystallized micritic matrix. The sample is dominated by abundant, large fragments of rudists (Ru) and other undetermined bivalves (Bi) and minor presence of benthic foraminifera [e.g., *Dicyclina* (Di) and miliolids (M)]. Common presence of subrounded micritic-rich intraclasts (In). Sample 22,020,402, Barranco de las Cuevas section; **d** Facies C3.2, Foraminiferal wackestone–mudstone and rudist rudstone–floatstone. Wackestone with locally recrystallized micritic matrix. The skeletal assemblage comprises abundant small benthic foraminifera (BF), rare large benthic foraminifera, ostracods (Os), and gastropod fragments (G). Sample 22,020,404, Barranco de las Cuevas section; **e** Facies C3.3, Fenestral dolo-mudstone. Mudstone with common fenestral porosity, occluded by medium-crystalline calcite; minor presence of very fine crystalline replacive dolomite. The skeletal grains are scarce, with small benthic foraminifera (BF), ostracods, and gastropod fragments. Sample 22,020,406, Barranco de las Cuevas section; **f** Facies C4.3, Calcareous sandstone. Fine-grained calcareous sandstone. Common micrite matrix with abundant fine-grained, subangular-to-angular quartz grains and minor phosphatic grains. Abundant echinoid (E), bivalve (Bi), and bryozoan (Br) fragments are also present. Sample 22030109A, Castroserracín section. See Fig. 2 for location and name of key sections

interpreted as related to sea levels markedly lower than those of the outer ramp facies (facies association A) (Barroso-Barcenilla et al. 2011).

Inner ramp facies association (C)

Four sub-associations are distinguished within the inner ramp: high-energy barrier (C1), low-energy lagoon (C2), carbonate tidal-flat (C3), and siliciclastic shoreface (C4). The carbonate inner ramp facies in thin-sections are mainly characterized by the presence of rudists, benthic foraminifera and dasycladacean green algae, and the absence of planktic foraminifera.

Four facies are distinguished within the high-energy barrier sub-association (C1): C1.1, cross-bedded bioclastic grainstone (Figs. 6e and 8d), C1.2, Massive, peloidal and foraminiferal packstone (Figs. 6f and 8e), C1.3, Rudist biostrome (boundstone) (Fig. 8f), and C1.4 Bioclastic and intraclastic packstone, with local rudstone and floatstone textures (Figs. 7a and 8g). The sub-association is characterized by the presence of rudists, benthic foraminifera, and coated grains. Oysters (pycnodonts, gryphaeas), serpulids, inoceramids, and planktic foraminifera are absent. The non-skeletal grains are mainly peloids. Bioturbation is rare to mainly absent.

This sub-association consists of rudist biostromes (Fig. 8f) and skeletal limestones, mostly of grainstone and packstone facies (Figs. 8d and e), but also rudstone, floatstone, and boundstone textures. It comprises a wide range of well to moderately sorted, skeletal-rich bioclastic limestones with rudists, foraminifera, and non-skeletal carbonate grains, such as peloids, intraclasts, and coated grains.

The grainstone facies (C1.1; Fig. 8d) with sharp erosional bases and cross-bedding indicate sedimentation in a shallow, high-energy inner ramp environment, above fair wave weather base and close to low tide level, at depths less than the packstone facies (C1.2 and C1.4). They likely originated from the migration of skeletal sand shoals. The lack of mud, the presence of coated grains, abraded bioclasts (Fig. 6e), cross-lamination, abundance of intraclasts and mud peloids, and generally well-sorted fabric indicate deposition in a relatively high-energy environment subjected to continual wave agitation (Tucker and Wright 1990; Flügel and Munnecke 2010).

The foraminiferal–peloidal packstone facies (C1.2) were deposited in a moderate-energy inner ramp setting (Fig. 8e). The presence of a rich benthic fauna with dominant foraminifera (Fig. 6f) and abundant peloids indicates a shallow environment. The occurrence of foraminifera indicates deposition in an inner ramp setting (Hohenegger 2000; Reiss and Hottinger 1984). The presence of dasycladacean algal debris in the granular facies is also characteristic of strong hydrodynamics. They are considered signs of significant sedimentary transport (Granier 2012). Most of the peloids with elongate and rod-like shapes likely correspond to fecal pellets (Flügel and Munnecke 2010), whereas other grains originated from the reworking of weakly lithified carbonate mud (i.e., mud peloids).

The rudist biostrome facies (C1.3; Fig. 8f) is interpreted as shallow, mostly subtidal, inner ramp deposit, showing a laterally and vertically patchy distribution of rudist beds. Rudists were adapted to substrates with positive sediment accumulation (elevators), which could develop into densely packed groups of individuals (Fig. 8f). The lack of mudstone sediment and foraminifers in the matrix, and the vertical succession of rudist fabrics suggest high hydrodynamic gradient settings, decreased sedimentation rates, high biological competition for (limited) available space, and shallowing-upward trends, even with subaerial exposure events (Gil et al. 2002, 2009).

The bioclastic and intraclastic packstone facies (C1.4; Figs. 7a and 8g) were deposited in an agitated, shallow-water inner ramp area, above fair-weather wave base, closely related to the skeletal grainstones (C1.1 facies). The microfacies show rudist bioclasts embedded in a fine-grained matrix, rich in other bivalves, benthic foraminifera, echinoids, bryozoans, and intraclasts (Fig. 7a). The high faunal diversity reflects deposition under normal salinity. C1.4

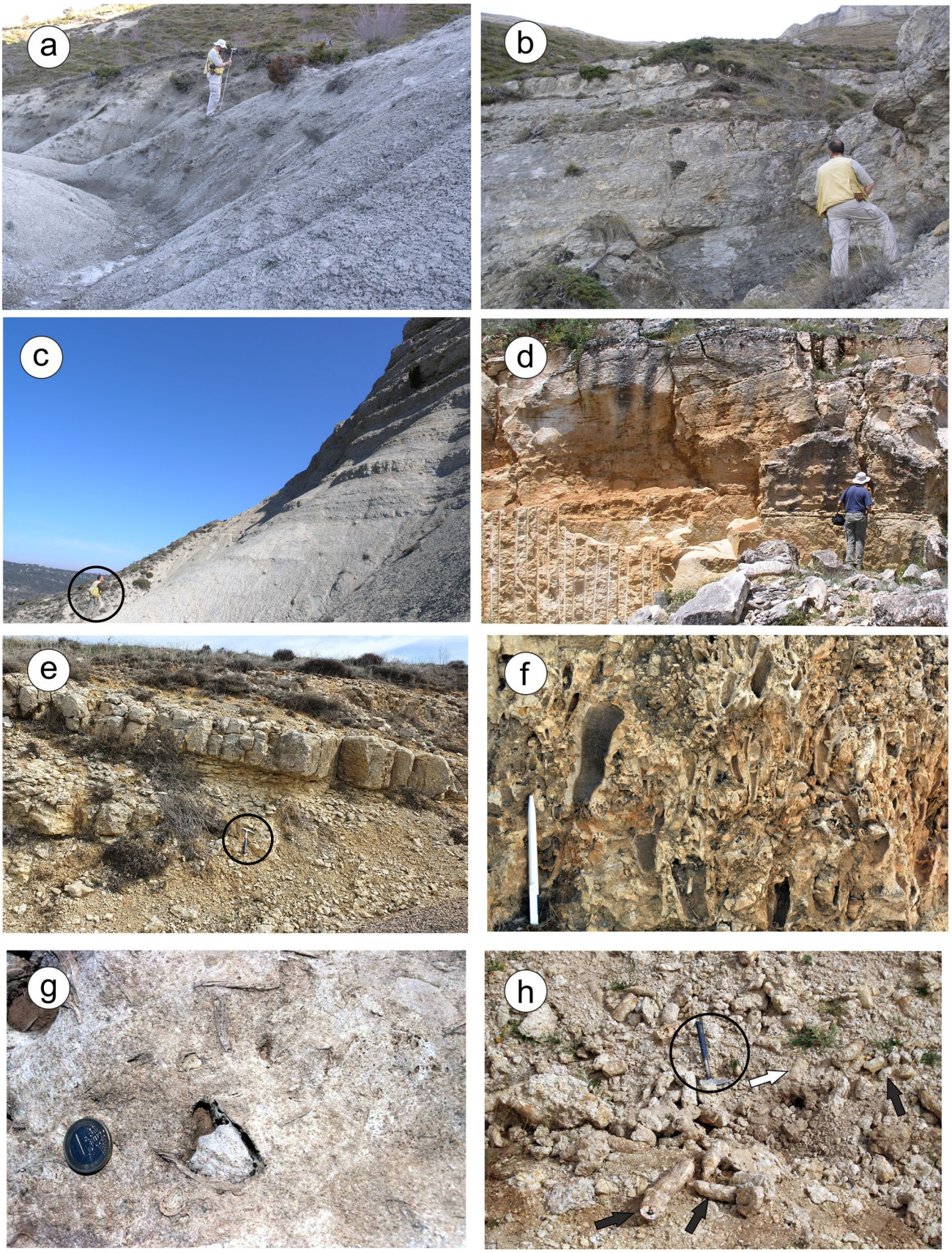
a
b
c
d
e
f
g
h

◂**Fig. 8** Field views of selected facies. **a** Facies A1, Marlstones, and calcareous marlstones. Dark-gray marlstones at the base of the middle member of Nidáguila Formation (see Fig. 2). Villamartín section. Height of person is 1.80 m tall; **b** Alternation of massive mudstones and wackestones (Facies A2) and laminated, peloidal wackestones (Facies A3). Upper part of the middle member of Nidáguila Formation at Villamartín section. Height of person is 1.80 m tall; **c** upper part of Turzo section showing the vertical transition between outer ramp (A) facies (below, middle member of Nidáguila Formation) and mid-ramp (B) facies (above, Nocedo de Burgos Formation). Height of person is 1.80 m tall (encircled, lower left); **d** Facies C1.1, Cross-bedded bioclastic grainstone at Castrojimeno section. Height of person is 1.80 m tall; **e** Facies C1.2, Peloidal and foraminiferal packstones at Castroserracín section. Hammer encircled for scale; **f** Facies C1.3, Rudist Biostrome (Boundstone) at Castrojimeno section. Oligospecific, closely packed, autochthonous frame reefs exclusively composed by rudist lower valves. Pen for scale is 12 cm long; **g** Facies C.1.4, bioclastic and intraclastic packstone, with abundant rudist and oyster bioclasts and common presence of moldic porosity by dissolution of inner molds of rudist lower valves (right of coin), Castrojimeno section; **h** Facies C2.2, Marly limestone and marlstone showing a parautochthonous spaced cluster reef of loose vaccinitids (black arrows) and isolated specimens in life position embedded in marlstone (white arrow), Castrojimeno section. Hammer encircled for scale. See Fig. 2 for location and name of key sections

facies were closely related to the peloidal and foraminifera packstones (C1.2). Both the C1.2 and C1.4 packstone facies show evidence of moderate-to-high-energy levels, including low mud content and moderate sorting. Floatstones-to-rudstones in C1.4 are mainly composed of reworked rudist and oyster (*Pycnodonte*) bioclasts, which are broken shells that show no grading or lamination (Fig. 8g). The common presence of broken shells and poorly sorted intraclasts suggests the occurrence of higher energy episodes above fair-weather wave base. They are derived from the erosion of C1.3 boundstones in nearby environments, likely by punctuated events (such as storms).

The lagoonal sub-association (C2) comprises thin/medium- to thick-bedded wackestones and marlstones. Bioclasts in this sub-association include rudists, other bivalves, green algae, echinoderms, gastropods, bryozoans, ostracods, and benthic foraminifera, especially miliolids. The non-skeletal grains are mainly peloids. C2 consists of two facies: C2.1, Burrowed, peloidal and foraminiferal wackestone (Fig. 7b), C2.2 Marly limestone and marlstone (Fig. 8h).

C2.1 is a back-barrier, lateral gradation of C1.2, with less energetic facies (wackestone) and burrowed in a protected environment with less energy (Fig. 7b). Marlstones rich in marine fauna (C2.2; Fig. 8h) also suggest a lagoonal setting within a low-energy subtidal area on a back-barrier area. The presence of a rudist-rich fauna in the marlstones indicates that a moderate amount of fine terrigenous input was not a primary control on the absence or presence of rudists, or on the components of the rudist assemblages. The morphology of articulated rudists within the floatstones suggests *in situ* conservation of reclining or forward-leaning organisms (Fig. 8h), which had to adapt to the continuous inflow of fine-grained sediments. Rudists (hippuritids and vaccinitids) are well adapted to life in muddy siliciclastic environments due to their filter-feeding mode of life and their capability for rapid upward growth (Steuber 1996), acquiring their typical elongate forms (Fig. 8h). The presence of disarticulated shells in C2.2 is probably related to storm events that remobilized soft-ground seafloors. There are also laterally extensive rudist biostromes (C1.3) intercalated within the lagoonal marlstones (C2.2). The presence of corals and chaetetids here also suggests a very shallow environment. The growth of these organisms was related to the rudists, as they developed in protected biostrome areas. In view of the high proportion of fine-grained siliciclastic input and, probably nutrients, the establishment of a permanent, compact rudist population was important. However, only short intervals of time were favorable for the colonization and growth of corals at the top of these rudist biostromes. Large areas with a soft substrate, either muddy or micritic (Fig. 8h), persisted (and became re-established after sporadic smothering of corals and rudists), favoring a bottom community with non-rudist bivalves, benthic foraminifera, gastropods, and minor echinoids (C2.1; Fig. 7b).

The lagoonal sub-association is marl dominated (C2.2; Fig. 8h). The presence of marlstones and the high proportion of micritic mud suggests deposition in a low-energy (calm) environment (Fürsich et al. 2003; Srivastava and Singh 2017). Peloidal and foraminiferal wackestone facies (C2.1, Fig. 7b) with a fine-grained muddy texture indicate widespread low-energy, subtidal lagoonal environments (Fürsich et al. 2003) next to the lower limit of fair-weather wave base, which is characterized by less turbulent conditions. The textural characteristics with the presence of micritic peloids of possible fecal origin, and the dominance of benthic foraminifera, bivalves, gastropods, and green algae (Fig. 7b), demonstrate a very shallow-marine, lagoonal environment, with relatively weak currents (Romero et al. 2002; Bádenas and Aurell 2010), but close to emergent shoals. The presence of shallow-water light-dependent organisms (Dasycladacean algae, large benthic foraminifera, and local corals) characterize shallow-water environments (Granier 2012), in an essentially protected inner ramp, lagoonal setting.

The shoreline margins of the basin were dominated by carbonate tidal flats (facies sub-association C3) that were widely developed in the farther southern areas of the basin. Siliciclastic input to shoreface environments, with limited extension, created a narrow siliciclastic shoreline facies belt (facies sub-association C4).

The carbonate tidal flats (C3) are characterized by the presence of microbial laminites, dolomites, and marlstones, with replacive dolomite/calcite and hardground development; meanwhile, detrital silt-size quartz grains are scarce.

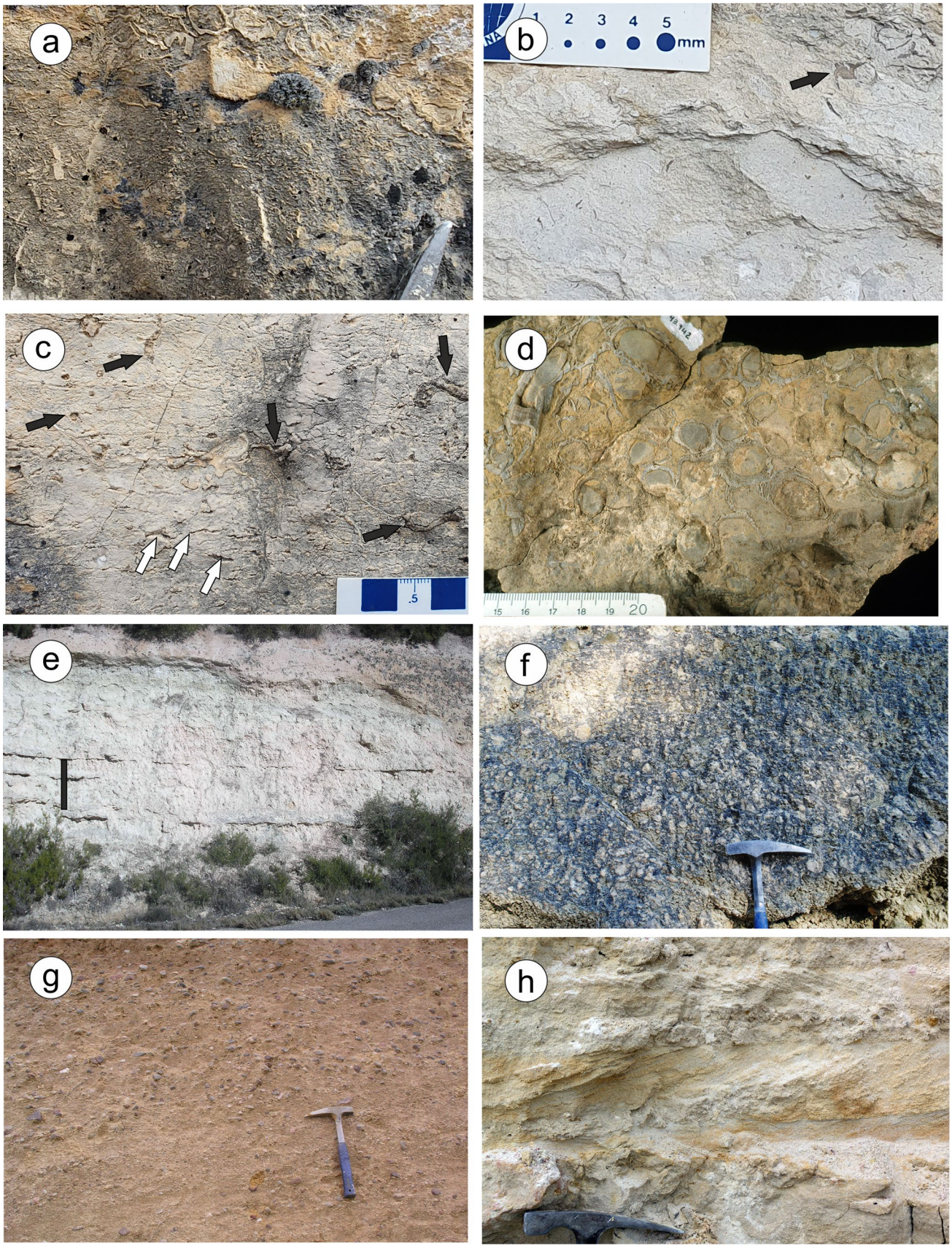
a
b
1 2 3 4 5 mm
c
.5
d
15 16 17 18 19 20
e
f
g
h

◂**Fig. 9** Field views of selected facies. **a** Facies C3.1, Rudist rudstone composed of poor sorted rudist debris with locally partially intact shells (upper part of the image). Barranco de las Cuevas section. The point of the hammer for scale is about 5 cm long; **b** Facies C3.2, Foraminiferal wackestone–mudstone and rudist rudstone–floatstone with rudist valves scarcely fragmented (floatstone) arrowed; **c** Facies C3.3, Fenestral argillaceous dolo-mudstone with an irregular mm-scale fenestral lamination (white arrows) and small burrows (black arrows). Scale in cm; **d** Facies C3.4, Rudist cluster. Monoespecific cluster reef of *Bournonia gardonica*. Barranco de las Cuevas section, sample PUAB 93942, palaeontological collections of the Universitat Autònoma de Barcelona (PUAB); **e** Facies C3.7, Beige dolomitic marlstone and green marlstone at Embalse de Entrepeñas section. Vertical black bar for scale is 0.5 m long; **f** Facies C3.8, Dolomitic breccia with vertical joints and chicken wire-like structures that give it a pseudonodular appearance. Embalse de Entrepeñas section; **g** Facies C4.1, Coarse sandstone and gravel with a subtle planar lamination and orientation of some elongated clasts. Valdeprados section: **h** Facies C4.2, Fine-grained sandstone with planar cross-bedding and appearance of herringbone cross-lamination. Sepúlveda section. See Fig. 2 for location and name of key sections

The C3 sub-association is subdivided into eight facies: C3.1, Rudist rudstone (Figs. 7c and 9a), C3.2, Foraminiferal wackestone-mudstone and rudist rudstone-floatstone (Figs. 7d and 9b), C3.3, Fenestral dolo-mudstone (Figs. 7e and 9c), C3.4, Rudist cluster (Fig. 9d), C3.5, Beige to red mudstone, claystone and marlstone, C3.6, Massive dolomite, C3.7, Beige dolomitic marlstone and green marlstone (Figs. 9e), and C3.8, Dolomitic breccia (Fig. 9f). The sub-association shows an overall lateral gradation from subtidal-intertidal limestones (C3.1 to C3.5) to inter-supratidal marlstones and dolomites (C3.6-to-C3.8).

In some areas, the vertical lithofacies organization consists of several meter-scale, shallowing-upward cycles with a hardground developed at the top of the cycles. Typical cycles comprise facies C3.1 (subtidal)–C3.2/C3.4 (subtidal)–C3.3 (intertidal)–C3.5 (inter-supratidal). Incomplete cycles lack facies C3.5. These cycles are usually bounded by hardground surfaces at the top of dolomitized fenestral mudstones (C3.3) when incomplete or red mudstones (C3.5) when complete.

The rudstones (C3.1; Fig. 9a) represent a distinctive lithology associated with foraminiferal wackestones–mudstones, rudist rudstones–floatstones (C3.2; Fig. 9b), and isolated rudist clusters (C3.4; Fig. 9d). The predominance of rudist fragments in the rudstones (C3.1; Fig. 9a) suggests that they originated from the transport and accumulation of rudist skeletal sands from the reworking of rudist clusters (C3.4; Fig. 9d). The coarser grain-size and texture suggest that C3.1 originated from high-energy, strong events, such as large waves or storms, that affected the tidal areas and accumulated rudist debris in subtidal areas. These rudists grew in areas of moderate-to-low water energy, such as subtidal settings of tidal flats close to sheltered lagoons (Sanders 1996; Moro 1997). The main difference between C1.3 (biostromes) and C3.4 (clusters) precisely is the size and length of rudist bodies. At the high-energy barrier area, the rudists may develop as extended, but thin, mainly biostromal reefs; meanwhile, in the tidal area, the rudists were small, isolated clusters. The wackestones–mudstones (C3.2; Fig. 9b) accumulated in a shallow subtidal environment of low-energy waters, as suggested by the common presence of a muddy matrix and fossils of quiet, shallow subtidal areas (e.g., benthic foraminifera, red and calcareous green algae; Fig. 7d) (Jacka and Brand 1977). The C3.2 rudstone–floatstone (Fig. 9b) consist of broken rudists fragments and foraminiferal tests, periodically eroded from clusters (facies C3.4; Fig. 9d) by storm and wave processes. The mudstones with fenestrae (C3.3; Fig. 7e) are interpreted as microbial mats (stromatolites; Fig. 9c) deposited in a protected intertidal area, probably at the border of a lagoon. The fenestral voids suggest deposition under meteoric and/or vadose influence (Flügel and Munnecke 2010). The low abundance and diversity of fauna support such an interpretation. The dominant sedimentary process in facies C3.5 was suspension settling (decantation), deposited in an intertidal–supratidal environment with a low hydrodynamic gradient, associated with episodes of low sedimentation rates and periodic input from nearby emergent areas. The presence of iron accumulation (reddening) in these facies suggests the development of sedimentary breaks under oxidizing conditions.

The southeastern end of the studied basin is composed of C3.6-to-C3.8 facies, with a local presence of C3.3 facies. The main facies in this area are green marlstones (C3.7; Fig. 9e); they are characterized by the presence of detrital illite and kaolinite, and medium-grained subangular quartz grains (Fernández Calvo 1982). Lithology and composition suggest that they were deposited on extensive, intertidal–supratidal mudflats with a predominance of emergent conditions and continental influence. Facies C3.6 (and C3.3) are locally intercalated within the green marlstones being interpreted as intertidal carbonates and stromatolites. Locally, there are dolomitic breccias with nodular aspect (Fig. 9f) and vertical joints (facies C3.8) that are interpreted as palaeosol dolocretes generated by *in situ* brecciation (Wright 1994) and caused by a combination of processes (Klappa 1980). Based on the fine-grained nature of the dolomite and the absence of skeletal grains, deposition probably occurred in a low-energy, restricted intertidal-to-supratidal environment (Wilmsen et al. 2010). Low faunal diversity most likely indicates the effect of high salinity.

The siliciclastic, shoreface facies (C4) are restricted to the shoreline areas of the emergent Massif; besides, a fringe of calcareous sandstones is also related to these sediments. Minor detrital, monocrystalline quartz grains are also commonly found mixed with carbonate sediments in several of the studied sections, mainly basinward (Fig. 3a). Three facies are distinguished: C4.1, Coarse sandstone and gravel (Fig. 9g), C4.2, Fine-grained sandstone (Fig. 9h), and C4.3, Calcareous sandstone (quartz-rich packstone; Fig. 7f).

The planar lamination in the coarse sandstone and gravel (C4.1, Fig. 9g) reflects plane bed transport. This action is capable of selectively sorting and uniformly spreading sediment into individual layers (Clifton 1969). Interbeds of sand and gravel are typical in upper shoreface–foreshore deposits (Pemberton et al. 2012). They indicate sediment deposition by alternating high- and low-energy flows. The gravel beds were probably deposited by high-energy flows during storms, whereas the sand beds would have to be laid down by lower-energy flows during waning storms or fair-weather conditions (Hiroki and Terasaka 2005). Cross-lamination in fine-grained sandstone (C4.2; Fig. 9h) characterizes low-regime tractive processes. The presence of cross-lamination results from the migration of small dunes with an abundant sand supply, and variable wave energy on the upper shoreface, above fair-weather wave base (e.g., Pemberton et al. 2012). Massive and parallel-laminated sands resulted from rapid sedimentation from suspension when large amounts of sand accumulated during moments of higher wave energy. The lateral continuity of sand beds, the high degree of sand sorting, the overall lack of fine-grained material, and the paucity of biogenic structures and fauna also suggest sedimentation under high-energy conditions in the shoreface of a coastal environment (Myrow et al. 2002), close to the palaeo-sea level (Seidler and Steel 2001). Evidence of tidal processes is recorded by the presence of herringbone cross-bedding (Fig. 9h).

These facies are interpreted as a prograding shoreface–foreshore system, representing a low-gradient, wave-dominated shoreline environment, with significant influences from storm and tidal processes. The presence of mixed siliciclastic–carbonate facies and siliciclastic grains within the carbonate facies throughout the studied area will be discussed further below.

The calcareous-sandstone facies (C4.3) display significant amounts of siliciclastic grains mixed with a large diversity of marine fauna (Fig. 7f). The generally good sorting and broken skeletal grains suggest the existence of frequent reworking by moderate and high-energy currents. The presence of an open-marine fauna, and planktic and benthic foraminifera indicate an open-marine depositional setting. The relationships with C1.4 and C4.2 facies suggest a lower shoreface and/or inner ramp setting with a large siliciclastic influence, close to fair-weather wave base.

Discussion and interpretation

The results described above have enabled us to improve the faunistic associations across the carbonate ramp and to revise the facies model of García-Hidalgo et al. (2012) and the palaeogeographic reconstruction of Callapez et al. (2015) by integrating new data on the sedimentary facies.

Faunistic associations

The most characteristic biogenic components are rudists and large benthic foraminifera (LBF). Other bivalves (oysters, pectinids, and inoceramids), bryozoans, echinoderms, gastropods, calcareous green algae, and ostracods are also abundant. Planktic foraminifera, ammonoids, and nautiloids are common in the outer ramp facies. It is remarkable the rare presence of corals, mainly limited to the lagoon and the protected areas in the shoals. The faunal distribution in the main facies and depositional environments is shown in Fig. 10.

The rudists, mainly radiolitids and hippuritids, were abundant from the subtidal to the shallow and energetic proximal inner ramp (Fig. 10). Intact rudist shells, biostromes, and thickets were commonly developed. Three main environments with autochthonous rudist fabrics, characterized by different hydrodynamic conditions, are distinguished: a) Rudist biostromes (boundstone; facies C1.3) occur near barrier, high-energy inner ramp. They are dominated by a conical-shaped, pauciespecific rudist-rich association, with very low to absent relief (Fig. 8f); b) Rudists embedded in marly limestones and marlstones in a low- to moderate-energy inner ramp (protected lagoon; facies C2.2). They are dominated by fine-grained siliciclastic-rich sediments, where rudists (hippuritids and vaccinitids) are multispecific (Fig. 8h). These rudists display a wide variety of external morphologies, ranging from conical, cylindrical-to-subcylindrical and flat and wide shapes, including huge, isolated elevator morphotypes; and finally, c) monospecific, small rudist clusters dominated by fine-grained carbonate-rich sediments (Facies C3.4; Fig. 9d). They are related to sedimentation in subtidal areas. High-energy hydrodynamic currents, probably related to waves and storm events, washed out the matrix support and reworked and fragmented rudist shells, creating floatstone and rudstone textures in these sub-environments (Facies C1.4, C3.1 and C3.2; Figs. 8g, 9a and 9b).

Benthic foraminifera comprise two informal groups: (1) small benthic foraminifera or micro-foraminifera, without complex wall structures and interpreted as not hosting photosynthetic symbionts. The lack of specific sunlight requirements allows these groups to occupy more diverse ecological niches, where they are abundant throughout the entire ramp, although less abundant in the outer ramp setting (Fig. 10). They are mostly represented by textulariids, ataxophragmiids, nezzazatinellids, discorbidae, and simple forms of miliolids and rotaliids. (2) Larger forms, referred to as macro-foraminifera or Larger Benthic Foraminifera (LBF), include: a) abundant agglutinated forms (*Cuneolina* spp., *Dicyclina schlumbergeri*, *Pseudocyclammina* spp., *Dictyopsella* sp., *Orbitolinopsis cf. senonicus*); b) minor porcelaneous forms (*Nummofallotia cretacea*, *Vidalina*,

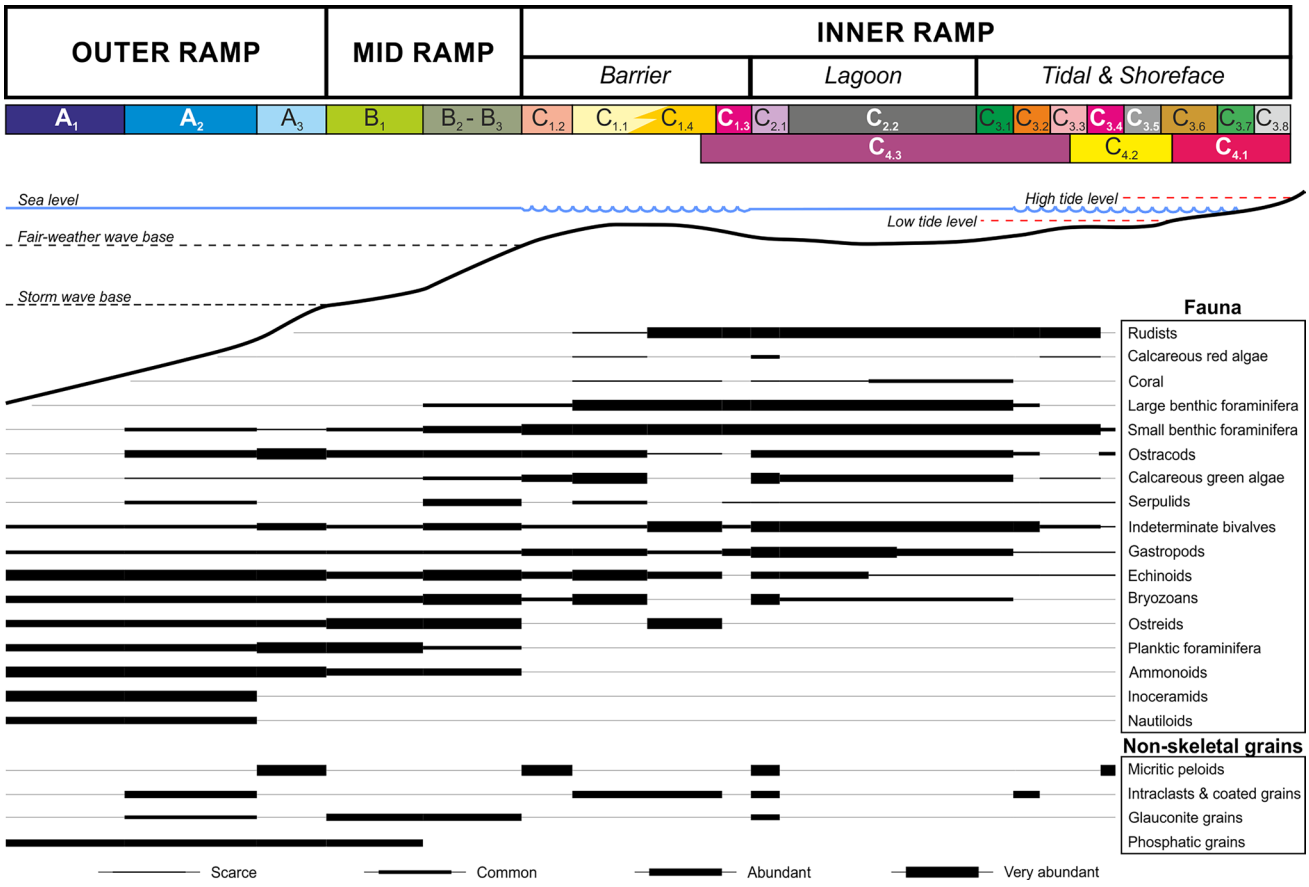

Fig. 10 Distribution of the main sedimentary environments on the Coniacian ramp, with the location of the different facies types (not to scale). The distribution of the main skeletal (fauna) and non-skeletal grains is also shown

Pseudonummoloculina?, *Scandonea?*), and c) less common hyaline forms (e.g., *Rotorbinella* spp.). The occurrence of larger porcelaneous foraminifera suggests sedimentation in a shallow-marine setting within the upper photic zone that corresponds to an inner ramp setting (Reiss and Hottinger 1984; Hohenegger 2000; Romero et al. 2002). In addition, LBF are interpreted to host photosynthetic, light-dependent symbiotic algae in their protoplasm, limiting their occurrence within the euphotic zone. Hence, the presence of LBF in the sediments is an important palaeobathymetric indicator of the photic zone (Fig. 10). LBF also reflect oligotrophic conditions in warm and shallow-water settings (Hallock and Glenn 1986). They are also used as biostratigraphic markers (e.g., Boix et al. 2011; Caus, et al. 2013; Albrich et al. 2014; Villalonga et al. 2019 from Pre-Pyrenees area). In this case, the presence of *Orbitilinopsis senonicus*, *Pseudocyclammina*, and *Rotorbinella* spp. would provide a low-confidence Coniacian-Lower Santonian age.

The faunal associations show a mixture of diverse sunlight-dependent (phototrophic) and nutrient-dependent (heterotrophic) organisms and may be considered either as a photozoan (James 1997; Michel et al. 2018) or a heterozoan carbonate association (Carannante et al. 1997; Schlager 2005; Brandano et al. 2009). However, the heterozoan interpretation is preferred because of the scarcity of corals and the overall sedimentary facies. Typically, heterozoan occurrences are found in basins with high nutrient influx and/or increased terrigenous material, which inhibit photozoan organisms and promote suspension-feeding organisms (e.g., bryozoans) in warm-water environments (Carannante et al. 1997; Philip and Gari 2005). A shoreline siliciclastic environment (facies C4) would provide terrigenous material (and probably nutrients) to the rest of the basin, as evidenced by the presence of mudstones in protected environments and quartz grains in several facies of the mid and outer ramp (Fig. 3). The terrigenous supply likely provided nutrients from the nearby emergent massif (Fig. 5). These nutrients, transported by longshore currents and then delivered to the basin, could have enhanced the development of suspension-feeding benthic organisms such as bivalves and bryozoans in deeper water environments and rudists in shallower ones (Philip and Gari 2005).

Vertical evolution and stacking patterns

The studied sediments show a transgressive–regressive depositional trend which is interpreted as a single third-order depositional sequence (García-Hidalgo et al. 2012). The vertical evolution and facies stacking patterns, with the distribution and shifting of facies and facies belts, are illustrated with three cross-sections (Figs. 3b, 4b and 5b) and maps of the depositional units (Fig. 11). The latter reflects three different palaeogeographical situations during the Coniacian, which are due to different relative sea levels, showing a trend of long-term transgression and final regression (Figs. 3 and 11).

The underlying Muñecas Formation (Fig. 3) ended with a significant drop in relative sea level, with exposure of many parts of the basin. The basal sequence boundary is either a hardground (Gil et al. 2006) or a dolomitic breccia (Floquet 1991). Basal deposits are represented mainly by inner and mid-ramp sediments (Facies B and C1; Fig. 11a). Toplap relationships with the underlying sequence (Gil et al. 2006), and the basal onlap and displacement of facies belts suggest a major sea-level fall at the sequence boundary followed by a rapid rise during the subsequent transgressive stage of this sequence. The siliciclastic coastal belt is also, locally, very extensive. The presence of quartz grains, at the base of the sequence, in several sections suggests a source to the ramp from shoreline siliciclastic environments (Sects. 3 and 5; Fig. 3a). Overlying these basal sediments, the sequence shows a sudden deepening with the appearance of outer platform marlstones and marlstone–limestone alternations in the northern sections (facies A, Sects. 1 to 4; Fig. 3b). A similar deepening-upwards trend within the Coniacian sediments also occurred in the Pyrenean Iberian margin (Andrieu et al. 2021).

The Coniacian ramp was a low-productivity system, similar to many other ramps (e.g., Burchette and Wright 1992), and drowned readily in response to sea-level rise due to its low topographic gradient. Then, the rapid flooding generated a landward migration and widening of the facies belts (Fig. 11b).

Maximum flooding extended the deeper sediments of the mid-outer ramp to the central part of the studied area (Figs. 3 and 11b). The maximum flooding surface (mfs) is, thus, recognized in the central area by the presence of Facies A1 in Sects. 5 to 7 (Fig. 3b); and by Facies A2 in Sects. 8 and 9 (Fig. 3b). In this area, the mfs represents the change between deepening upward to shallowing-upward, and from retrogradation to progradation (Fig. 3b). The presence of ammonites and nautiloids in Facies A2 within these sections also supports such an interpretation (Fig. 3a). In the northwest (outer ramp) area, the mfs is difficult to locate. It is contained at the base of the *Hemitissotia spp*. biozone, in a relatively thick interval characterized by a predominance of finer, outer ramp deposits (Facies A1 and A2; Fig. 3b). Consequently, at the maximum flooding, siliciclastic belts show the most limited extension (Fig. 11b).

Finally, the regressive sediments (Fig. 11c) show important facies aggradation and progradation of the mid- and inner ramp sediments with progradation of the siliciclastic facies belts (Figs. 4b and 5b). Carbonate development reached a maximum at this stage and is mainly associated with bioclastic wackestones and packstones of the mid ramp and peloidal and foraminiferal packstones of the inner ramp (Figs. 3 and 11c). The important accumulation in thickness of these facies produced a steeper ramp morphology that resulted in the change from a homoclinal ramp to a distally steepened ramp. This distally steepened ramp shows interfingering facies belts comprising highly productive bioclastic mid-ramp and diverse bioclastic inner ramp sediments. These deposits are characterized by low slope angles and a progradational to aggradational stacking pattern (Figs. 3b and 11c), typical of greenhouse ramps (Read 1998). The maximum regressive surface of the upper sequence boundary is marked by minor episodes of subaerial exposure with a rapid, although less pronounced, change in the vertical facies trend (first described by Floquet 1991).

Siliciclastic deposits and carbonate-siliciclastic facies mixing

Mixed siliciclastic–carbonate systems are widely distributed throughout the peri-Tethyan domain. They can be found from the west Portuguese basin (Segura et al. 2014), the central Iberia (e.g., Floquet 1991; Gil et al. 2006, and this work), the Pyrenean Iberian margin (Andrieu et al. 2021), the Bohemian and Rhenian Massifs on the Mid-European island (e.g., Ulicny et al. 2009; Niebuhr et al. 2011), other northern European massifs (Andrieu et al. 2016), the northern calcareous Alps (e.g., Sanders and Pons 1999), the southern passive continental margin of present-day North Africa and Middle East (e.g., Bachmann and Kuss 1998; El-Azabi and El-Araby 2007; Powell and Moh'd 2011), and even India and the Himalayas (e.g., Sarkar et al. 2014; Zhang et al. 2004). The predominance of siliciclastics in shoreline facies belts indicates a persistent sediment supply from fluvial systems that drained from the emergent parts of nearby hinterlands (Tucker 2003). Sediment supply is undoubtedly a major external control on shelf growth, architecture, and potential to produce shelf sandstones (Tucker 2003; Carvajal et al. 2009). Given sufficient sediment supply, shoreline siliciclastics are capable of prograding to the shelf edge (e.g., Porębski and Steel 2006).

In many sedimentological studies, however, the role of sediment supply in mixed systems tends to be overlooked (Carvajal et al. 2009). Starvation and storage of clastics in nearshore environments are usually envisaged as common

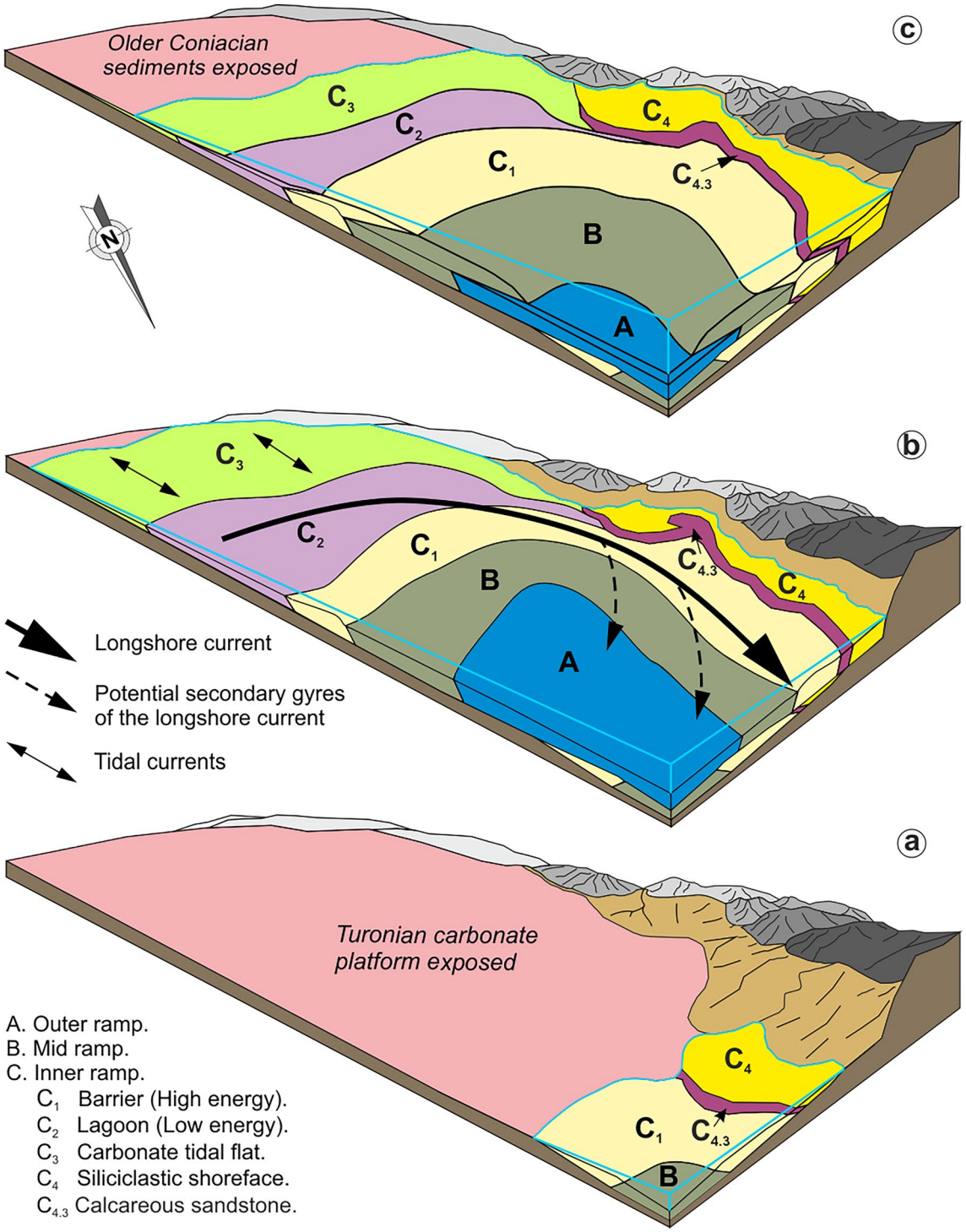

Fig. 11 Palaeogeographic reconstructions of the Coniacian platform, showing the distribution of the different environments and sub-environments during the three stages of the ramp evolution: **a** basal transgressive stage; **b** maximum flooding stage, and **c.** regressive stage. Local patterns of marine palaeocurrents are also shown at the maximum flooding (for figure clarity), but they were also active during the other stages of the ramp evolution

in these systems (Niebuhr et al. 2011). Nevertheless, even in microtidal environments, the calculated wave base is relatively deep (e.g., at the current Abu Qir Bay, Egypt, the wave base ranges between 16 and 29 m in depth with an average of 20 m; Frihy et al. 2008). This wave base is well below those depths at which shoreface siliciclastics and carbonate

sediments are usually considered to develop (e.g., El-Azabi and El-Arabi 2007). This shows that sand transport might occur deeper than previously considered, suggesting that the reworking and transporting of sand onto the shelf should have been more intensive than hitherto considered.

A problem arises when one considers why these sands sourced to the shoreline from emergent massifs were not redistributed rapidly and more widely across the shallower parts of a carbonate platform, considering the energetic processes occurring in these environments. These energetic processes potentially involve a combination of storm, wave and tidal currents. During storms, the combined action of waves and winds tends to create offshore-directed currents that move sediment to the shelf (Wright et al. 1991; Héquette et al. 2001). In contrast, under fair-weather conditions, smaller waves tend to transport sediment onshore; but contrary to what might be expected, low-frequency fluxes have been just as frequent onshore as offshore (Wright et al. 1991). Therefore, under appropriate conditions sand distribution across shallow shelves would be expected to occur more frequently.

In the case of the studied ramp, the predominance of siliciclastics in the shoreline facies belt indicates a persistent supply from fluvial systems that drained the emergent parts of the Iberian massif at the west (Figs. 4 and 5). It appears that the energy level was sufficient for the transportation and deposition of sand, and locally gravels, and for the progradation of a shoreface/foreshore system during the upper regressive deposits (Fig. 5). Significant amounts of sand were transported to the shoreline and mainly remained there, confined to the coastal belt. The transition from siliciclastic to carbonates occurred over short distances (Figs. 5 and 11). The zone of complete facies mixing, represented by the mixed calcareous-sandstone facies (C4.3), is restricted to an area about a few tens of kilometers wide (Figs. 5 and 11), which is similar to other modern basins (e.g., Neogene of Florida; McNeill et al. 2004). Thus, there seems to be a physical obstacle that: 1) keeps the sands close to the shoreline, as a coastal facies belt, 2) prevents their dispersion to the basin, and 3) impedes the facies mixing with the local development of a narrow belt of mixed facies (Fig. 11). It is suggested here that such a physical obstacle could be a longshore current flowing parallel to the coasts of the massif (Fig. 11). The presence of such a current must have caused, first, a grain-size segregation of sediments, and a clear separation of coarse-grained (coastal sands) from fine-grained facies (ramp muds and silts). Second, the sediment movement parallel to the coast, created by these currents, would have contributed to the long-term preservation of sands in shoreline region, impeding sand transport to the ramp, whereas the dispersion of muds and silts for greater distances would account for the prevalence of fine-grained strata in the mid and outer ramp. Besides, the ramp area was maintained as a main carbonate environment, with only a very narrow belt of true mixed facies.

The presence of sand within carbonates, however, is not uniformly distributed along the studied areas, some sections contain sand, and others are devoid of it. Thus, the Sepulveda section (10, Figs. 3a and 5) shows a notable sand input into the basin. It is significant that one area showed such a substantial and permanent proportion of sand input to the ramp over time. This constant input along the entire sequence cannot be interpreted as reciprocal sedimentation. The studied sections southwards, however, are completely devoid of sand (Figs. 3 and 4). On the contrary, northwards, sand content is progressively decreasing. First, close to the main siliciclastic source, sand-rich packstones (Facies C4.3) occur in Sect. 9 (Fig. 3a). Second, only minor, fine quartz grains are contained within the carbonates in sections even farther northwest (3, 5 and 6; Fig. 3a). Assuming this distribution of sand and the presence of a longshore current, this current should be an NW-flowing current (Fig. 11b). An NW-flowing current likely impeded the transport of large amounts of sand to the southeast (Figs. 3a and 4), where carbonate tidal flats were the dominant environments (12 and 13, Fig. 3b). The claystones and mudstones, as part of the tidal deposits, were probably sourced from nearby emergent low-lying areas at the closed end of the Iberian basin (Fig. 11).

Finally, conditions must have existed for minor sand transport from shoreline and mixed belts into a predominantly carbonate setting. This transport is minor and occasional for the sand grains, but is more important for the muddy particles that form the marlstones in the mid and outer ramp areas. Lagoonal marlstones, on the contrary, were probably sourced from the continental and tidal areas at the southeastern end of the basin. The influx and redistribution of siliciclastics are assumed to affect the production of carbonate sediments mainly by increasing water turbidity. In addition, these sediments may continually cover parts of the substrate and the related carbonate biotic assemblages, affecting carbonate production. However, except for the pure siliciclastic facies, virtually all facies contain skeletal components, non-skeletal grains (peloids), and/or carbonate mud (micritic matrix), which points to a continuously active carbonate factory in the ramp. In this system, terrigenous materials only reduce the carbonate sediments but do not interrupt the carbonate factory.

Implications for palaeogeography and palaeoceanography: winds and currents

The Iberian basin was located in the near-tropical and subtropical zones during Coniacian times (25–30ºN, Fig. 12; Andrieu et al. 2021). At these latitudes, the climate models and simulations for Late Cretaceous times (Hay 2008)

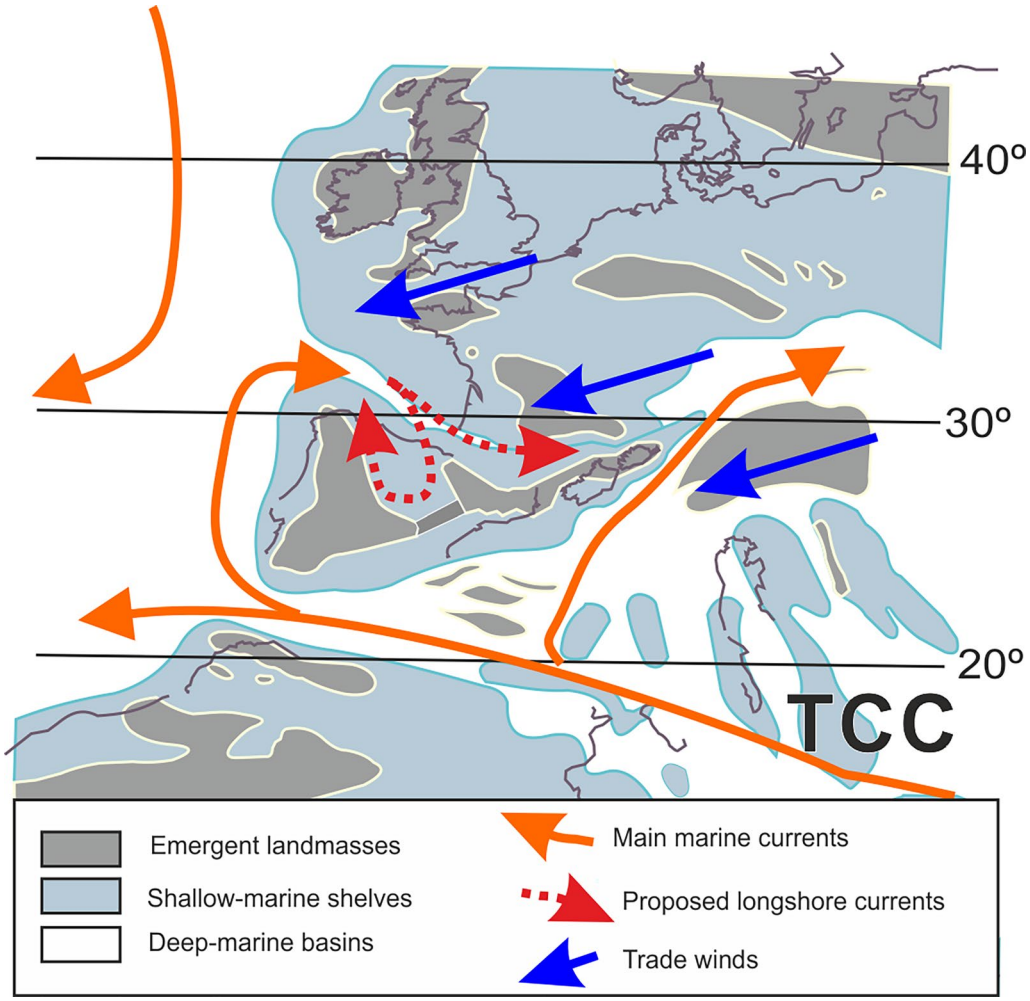

Fig. 12 Palaeo-oceanographic reconstruction of global and local current patterns around and within the Iberian microplate. Suggested trade winds are also shown; TCC, Tethyan Circumglobal Current. Modified from Callapez et al. (2015)

suggest the presence of tropical, easterly winds that persisted continuously throughout the year (blue arrows in Fig. 12). Wind blowing from the Iberian massif might be another potential mechanism for siliciclastic transport and distribution over large sectors of the basin. At the mentioned latitudes, however, the dominant winds were most likely directed toward the west and southwest (Hay 2008), as the current trade winds. Hence, the main winds should have blown toward the massif (not from the massif) inhibiting the sourcing of sand by wind from the Iberian massif to the basin (Fig. 12).

The proposed longshore current could have been induced from various processes, including tides, winds, and storms. Such currents within semi-enclosed basins are common in the marine realm (e.g., Adriatic, Poulain 2001; Arabian Gulf, Kämpf and Sadrinasab 2006). In the Iberian basin, longshore circulation was most likely induced by both the presence of external currents and wind-driven currents (Fig. 12).

The presence of an external current is necessary, because it allowed the entry and dispersal of invertebrate larvae from the Tethyan realm, where they originated and evolved (Callapez et al. 2015). This current was likely related to the oceanic circulation pattern around the Iberian microplate, which, in turn, was related to the Tethys Circumglobal Current (TCC) (Pucéat et al. 2005; Callapez et al. 2015). TCC is a westward surficial current toward the central Atlantic in the southern margin of the Iberian microplate (Barron and Peterson 1989; Kutzbach et al. 1990) (Fig. 12). Models also suggest that TCC was probably related to the development of one or more large gyres (Poulsen et al. 1998; Johnson 1999). These gyres would have caused a clockwise flow around Iberia (Callapez et al. 2015) and within the Iberian basin (Fig. 12).

On the other hand, wind-driven currents might be another factor influencing sediment transport across shallow-marine shelves. These currents can be drivers of sediment transport,

mainly wind-driven coastal flows during storms or tidal currents. Moreover, even in the presence of tidal currents, the sediment could be mainly transported alongshore (Héquette et al. 2008). The direction of sediment transport is mostly determined by the asymmetry of the flows, but wind forcing may also affect the current velocity by reinforcing or limiting it, depending on the concordance of wind and current direction (Héquette et al. 2008). It also causes near-bottom currents that affect sand movement (Guerrero et al. 2018). In this case, there is a clear concordance between wind direction and the presumed longshore current direction (Fig. 12), making probable the presence and reinforcement of such currents. External- and wind-driven currents, with clockwise gyres, would likely have generated a longshore current, parallel to the Iberian massif coast, which moved siliciclastic sediments to the NW, explaining the previously described sandy distribution and the observed pattern within the mixed siliciclastics and carbonates (Fig. 12).

Finally, the presence of phosphatic grains in the external parts of the ramp (mid-to-outer ramp) could be evidence of local upwelling sourced to the basin through the inflow of these external currents (Fig. 12). The presence of dark, massive marlstones with very poor macro-benthos in the outer ramp likely indicates the local presence of oxygen-poor bottom waters, related to this inflow (Fig. 12). This restricted environment could have been a source of episodic nutrient-rich waters from the deep ramp to the inner ramp, being another nutrient source for heterozoan organisms.

Conclusions

The Coniacian sediments of the Iberian basin are interpreted as a homoclinal ramp grading upwards into a distally steepened ramp. Meanwhile, the southwestern margin of the basin contains a coastal siliciclastic belt, the deposits of which were sourced from the emergent Iberian massif. Twenty-three facies were recognized and grouped into three main depositional environments: outer ramp, mid ramp, and inner ramp. Four different sub-associations were further distinguished in the inner ramp: barrier (shoal), lagoon, carbonate-tidal flat, and shoreface.

The most characteristic biogenic components show a mixture of large benthic foraminifera and rudists (among others), with a remarkable rare occurrence of corals. This association is a heterozoan carbonate association that thrived with increased terrigenous and/or nutrient influx. Three main sub-environments with autochthonous rudist fabrics, characterized by different hydrodynamic conditions, are also distinguished: a) rudist biostromes (boundstones) related to a near barrier, high-energy inner ramp; b) rudists embedded in marly limestones and marlstones in a low- to moderate-energy inner ramp (protected lagoon), and c) monospecific rudist clusters dominated by fine-grained carbonate-rich sediments, associated with sedimentation on the subtidal areas.

Sedimentation in the basin resulted from two distinct sedimentary systems: an NW–SE carbonate ramp and a fringe of siliciclastic sediments bordering the emergent Iberian massif. The former reflects a basinward decrease in energy gradients with the shallower, tidal facies developed in the extreme southeast of the basin. The nutrients provided by these siliciclastics promoted the development of heterozoan organisms. Three main stages of ramp evolution are distinguished: (1) transgressive, homoclinal ramp with a belt of shoreline siliciclastic sediments; (2) drowning and outer ramp widening with siliciclastic sediments, characterized by the predominance of finer, outer ramp deposits in the central parts of the basin, and lagoon and shoals in the inner ramp; (3) distally steepened ramp with facies aggradation and progradation of mid- and inner ramp sediments, with progradation of the siliciclastic coastal belt.

The siliciclastic facies distribution along the basin consisted of a major siliciclastic facies belt; a narrow, mixed belt of siliciclastic and carbonate grains; and minor sand grains dispersed within carbonate sediments, not affecting the carbonate factory. This distribution is problematic since sands sourced to the basin would be expected to have been redistributed rapidly and widely across the basin, considering the common storm, wave, and tidal processes shown by the sedimentary facies (both siliciclastics and carbonates). A longshore current flowing N and NW, parallel to the shoreline, is proposed to have been the process behind this siliciclastic sediment distribution.

The longshore current was likely induced both by external and wind-driven currents. A clockwise circulation is derived mainly from sand distribution among studied sections and was probably related to the oceanic circulation pattern around the Iberian microplate. These clockwise gyres facilitated larval dispersion to the enclosed Iberian basin and the local presence of upwelling, as shown by the presence of phosphatic grains in the mid-to-outer ramp. The upwelling of bottom waters could have been a minor, secondary source of episodic nutrient-rich waters from the deep ramp, which may also explain the development of heterozoan organisms even in the more proximal and relatively shallow-water facies.

Acknowledgements Field work began in 2009, being mainly funded by the Spanish projects CGL2009-12008 (DGICYT, Ministerio de Educación y Ciencia), PAI11-0237-7926, PEII-2014-037-P (Junta de Comunidades de Castilla–La Mancha), and PGC2018-101575-B-I00 (Ministerio de Ciencia, Innovación y Universidades). The authors would like to thank M. Segura and F. Barroso-Barcenilla for their help in earlier field works. The paper has benefited gratefully from the insight and by critical reviews of the Editor-in-Chief (Dr. Maurice Tucker), and M. El-Azabi and S. Andrieu whose valuable suggestions and their critical comments have allowed to improve an earlier version of this manuscript.

Author contributions All authors contributed to the study conception and fieldwork. Stratigraphic data and analysis, and sample collection were mainly performed by Javier Gil-Gil and Antonio Bretones. Sedimentological analysis was mainly performed by José F. García-Hidalgo. Thin-section study and microfacies analysis were performed by Carme Boix. The first draft of the manuscript was written by José F. García-Hidalgo and all authors commented on previous versions of the manuscript. All authors read and approved the final manuscript.

Funding Open Access funding provided thanks to the CRUE-CSIC agreement with Springer Nature.

Data availability The authors declare that the data supporting the findings of this study are available within this paper.

Declarations

Conflict of interest The authors declare that they have no known competing financial interests or personal relationships that could have appeared to influence the work reported in this paper.

References

Albrich S, Frijia G, Parente M, Caus E (2014) The evolution of the earliest representatives of the genus orbitoides: implications for upper cretaceous biostratigraphy. Cretac Res 51:22–34. https://doi.org/10.1016/j.cretres.2014.04.013

Andrieu S, Brigaud B, Barbarand J, Lasseur E, Saucède T (2016) Disentangling the control of tectonics, eustasy, trophic conditions and climate on shallow-marine carbonate production during the Aalenian-Oxfordian interval: From the western France platform to the western Tethyan domain. Sed Geol 345:54–84. https://doi.org/10.1016/j.sedgeo.2016.09.005

Andrieu S, Saspiturry N, Lartigau M, Issautier B, Angrand P, Lasseur E (2021) Large-scale vertical movements in Cenomanian to Santonian carbonate platform in Iberia: indicators of a Coniacian pre-orogenic compressive stress. BSGF. https://doi.org/10.1051/bsgf/2021011

Bachmann M, Kuss J (1998) The Middle Cretaceous carbonate ramp of the northern Sinai: sequence stratigraphy and facies distribution. Geol Soc London, Spec Publ 149:253–280. https://doi.org/10.1144/GSL.SP.1999.149.01.13

Bádenas B, Aurell M (2010) Facies models of a shallow-water carbonate ramp based on distribution of non-skeletal grains (Kimmeridgian, Spain). Facies 56:89–110. https://doi.org/10.1007/s10347-009-0199-z

Barron EJ, Peterson WH (1989) Model simulation of the cretaceous ocean circulation. Science 244:684–686. https://doi.org/10.1126/science.244.4905.684

Barroso-Barcenilla F, Callapez PM, Ferreira Soares A, Segura M (2011) Cephalopod assemblages and depositional sequences from the upper Cenomanian and lower Turonian of the Iberian Peninsula (Spain and Portugal). J Iberian Geol 37:9–28. https://doi.org/10.5209/rev_JIGE.2011.v37.n1.1

Boix C, Frijia G, Vicedo V, Bernaus JM, Di Lucia M, Parente M, Caus E (2011) Larger foraminifera distribution and strontium isotope stratigraphy of the La Cova limestones (Coniacian–Santonian, "Serra del Montsec", Pyrenees, NE Spain). Cretac Res 32:806–822. https://doi.org/10.1016/j.cretres.2011.05.009

Brandano M, Frezza V, Tomassetti L, Cuffaro M (2009) Heterozoan carbonates in oligotrophic tropical waters: The Attard member of the lower coralline limestone formation (Upper Oligocene, Malta). Palaeogeogr Palaeoclimatol Palaeoecol 274:54–63. https://doi.org/10.1016/j.palaeo.2008.12.018

Burchette TP, Wright VP (1992) Carbonate ramp depositional systems. Sed Geol 79:3–57. https://doi.org/10.1016/0037-0738(92)90003-A

Callapez PM, Gil Gil J, García-Hidalgo JF, Segura M, Barroso-Barcenilla F, Carenas B (2015) The Tethyan oyster Pycnodonte (Costeina) costei (Coquand, 1869) in the Coniacian (Upper Cretaceous) of the Iberian Basin (Spain): Taxonomic, palaeoecological and palaeobiogeographical implications. Palaeogeogr Palaeoclimatol Palaeoecol 435:105–117. https://doi.org/10.1016/j.palaeo.2015.05.011

Campbell AE (2005) Shelf-geometry response to changes in relative sea level on a mixed carbonate–siliciclastic shelf in the Guyana Basin. Sed Geol 175:259–275. https://doi.org/10.1016/j.sedgeo.2004.09.003

Carannante G, Graziano R, Ruberti D, Simone L (1997) Upper Cretaceous temperate-type open shelves from northern (Sardinia) and southern (Apennines-Apulia) Mesozoic Tethyan Margins. In: James NP, Clarke JAD (eds) Cool-water carbonates. SEPM, Berlin

Carson GA, Crowley SF (1993) The glauconite-phosphate association in hardgrounds: examples from the Cenomanian of Devon, southwest England. Cretac Res 14:69–89. https://doi.org/10.1006/cres.1993.1006

Carvajal C, Steel R, Petter A (2009) Sediment supply: The main driver of shelf-margin growth. Earth-Sci Rev 96:221–248. https://doi.org/10.1016/j.earscirev.2009.06.008

Catuneanu O, Galloway WE, Kendall CGSC, Miall AD, Posamentier HW, Strasser A, Tucker ME (2011) Sequence stratigraphy: methodology and nomenclature. Newsl Stratigr 44(3):173–245. https://doi.org/10.1127/0078-0421/2011/0011

Caus E, Parente M, Vicedo V, Frijia G, Martínez R (2013) Broeckina gassoensis sp. nov., a larger foraminiferal index fossil for the middle Coniacian shallow-water deposits of the Pyrenean Basin (NE Spain). Cretac Res 45:76–90. https://doi.org/10.1016/j.cretres.2013.08.002

Christ N, Immenhauser A, Amour F, Mutti M, Tomás S, Agar SM, Always R, Kabiri L (2012) Characterization and interpretation of discontinuity surfaces in a Jurassic ramp setting (High Atlas, Morocco). Sedimentology 59:249–290. https://doi.org/10.1111/j.1365-3091.2011.01251.x

Clifton HE (1969) Beach lamination: nature and origin. Mar Geol 7:553–559. https://doi.org/10.1016/0025-3227(69)90023-1

Dunham RJ (1962) Classification of Carbonate Rocks According to Depositional Texture. In: Ham WE (ed) Classification of Carbonate Rocks. AAPG, Tulsa

El-Azabi MH, El-Araby A (2007) Depositional framework and sequence stratigraphic aspects of the Coniacian-Santonian mixed siliciclastic/carbonate Matulla sediments in Nezzazat and Ekma blocks, gulf of Suez. Egypt J of African Earth Sci 47:179–202. https://doi.org/10.1016/j.jafrearsci.2007.02.002

Embry AF, Klovan JE (1971) A Late Devonian reef tract on Northeastern Banks Island, NWT. Can Petrol Geol Bull 19:730–781. https://doi.org/10.35767/gscpgbull.19.4.730

Fernández Calvo, C (1982): Sedimentología y diagénesis del Cretácico superior de La Mancha (provincia de Cuenca). PhD Thesis. Departamento de Petrología. Facultad de Ciencias Geológicas. Universidad Complutense de Madrid.

Floquet M (1998) Outcrop cycle stratigraphy of shallow ramp deposits: the Late Cretaceous series on the Castilian ramp (northern Spain). In: De Graciansky PC, Hardenbol J, Jacquin T, Vail PR (eds) Mesozoic and Cenozoic Sequence Stratigraphy of European Basins. SEPM, Berlin

Floquet M, Alonso A, Meléndez A (1982) Cameros Castilla. El Cretácico superior. In: García A (ed) El Cretácico de España. Editorial Complutense, Madrid

Floquet M (1991) La plate-forme Nord-Castellane au Crétacé supérieur (Espagne). These. Memoires Geologiques de l'Université de Dijon, 14, pp 925

Flügel E, Munnecke A (2010) Microfacies of carbonate rocks analysis, interpretation and application, 2nd edn. Springer-Verlag, Berlin, Heidelberg

Frihy OE, Hassan MS, Deabes EA, Abd El Moniem AB (2008) Seasonal wave changes and the morphodynamic response of the beach-inner shelf of Abu Qir Bay, Mediterranean coast. Egypt Mar Geol 247:145–158. https://doi.org/10.1016/j.margeo.2007.09.001

Fürsich FT, Wilmsen M, Seyed-Emami K, Schairer G, Majidifard MR (2003) Platform-basin transect of a Middle to Late Jurassic large-scale carbonate platform system (Shotori Mountains, Tabas area, east-central Iran). Facies 48:171–198. https://doi.org/10.1007/BF02667538

Gallemí J, López G, Martínez R, Pons JM (2007) Macrofauna of the Villamartín section: Coniacian/Santonian boundary. North Castilian Platform, Burgos, Spain

García A, Mas R, Segura M, Carenas B, García-Hidalgo JF, Gil J, Alonso A, Aurell M, Bádenas B, Benito MI, Meléndez A, Salas R (2004) Segunda fase de post – rifting: Cretácico Superior. In: Vera JA (ed) Geología de España. Soc Geol España – Inst Geol y Min España, Madrid

García-Hidalgo JF, Barroso-Barcenilla F, Gil-Gil J, Martínez R, Pons JM, Segura M (2012) Stratal, sedimentary and faunal relationships in the Coniacian 3rd-order sequence of the Iberian Basin, Spain. Cretac Res 34:268–283. https://doi.org/10.1016/j.cretres.2011.11.007

Gil J, Pons JM, Segura M (2002) Redescripción de Bournonia gardonica (Toucas, 1907) (Radiolitidae, Bivalvia) y análisis de las facies en que aparece (Coniaciense, Sistema Central, España). Rev Esp Palaeontol 17:245–256

Gil J, Carenas B, Segura M, García-Hidalgo JF, García A (2004) Revisión y correlación de las unidades litoestratigráficas del Cretácico Superior en la región central y oriental de España. Rev Soc Geol España 17:249–266

Gil J, García-Hidalgo JF, Segura M, García A, Carenas B (2006) Stratigraphic architecture, palaeogeography and sea-level changes of a third order depositional sequence: The late Turonian–early Coniacian in the northern Iberian Ranges and Central System (Spain). Sed Geol 191:191–225. https://doi.org/10.1016/j.sedgeo.2006.03.023

Gil J, García-Hidalgo JF, Mateos R, Segura M (2009) Succession of rudistid lithosomes along the western coastal margin of the Iberian Basin (Coniacian, Castrojimeno section, central Spain). Facies 55:523–539

Gil J, García-Hidalgo JF, Segura M, Lopez Olmedo F, García A, Díaz de Neira A, Montes M, Nozal F (2010) El Cretácico del sistema central (españa): registro estratigráfico, contexto deposicional y esquema evolutivo. Bol R Soc Esp Hist Nat (sec Geol) 104:15–36

Gil J, Pons JM, Vicens E, García-Hidalgo JF, Segura M (2024) The turonian-campanian rudist bivalve succession in the central Iberian basin. Cretac Res. https://doi.org/10.1016/j.cretres.2023.105815

Granier B (2012) The contribution of calcareous green algae to the production of limestones: a review. Geodiversitas 34:35–60. https://doi.org/10.5252/g2012n1a3

Guerrero Q, Guillén J, Durán R, Urgeles R (2018) Contemporary genesis of sand ridges in a tideless erosional shoreface. Mar Geol 395:219–233. https://doi.org/10.1016/j.margeo.2017.10.002

Hallock P, Glenn EC (1986) Larger foraminifera: A tool for palaeoenvironmental analysis of Cenozoic carbonate depositional facies. Palaios 1:55–64. https://doi.org/10.2307/3514459

Hay WW (2008) Evolving ideas about the Cretaceous climate and ocean circulation. Cretac Res 29:725–753. https://doi.org/10.1016/j.cretres.2008.05.025

Héquette A, Desrosiers M, Hill PR, Forbes DL (2001) The influence of coastal morphology on shoreface sediment transport under storm-combined flows, Canadian Beaufort Sea. J Coast Res 17:507–516

Héquette A, Hemdane Y, Anthony EJ (2008) Sediment transport under wave and current combined flows on a tide-dominated shoreface, northern coast of France. Mar Geol 249:226–242. https://doi.org/10.1016/j.margeo.2007.12.003

Hillgärtner H (1998) Discontinuity surfaces on a shallow-marine carbonate platform(Berriasian, Valanginian, France and Switzerland). J Sed Res 68:1093–1108. https://doi.org/10.2110/jsr.68.1093

Hiroki Y, Terasaka T (2005) Wavy lamination in a mixed sand and gravel foreshore facies of the Pleistocene Hosoya Sandstone, Aichi, central Japan. Sedimentology 52:65–75. https://doi.org/10.1111/j.1365-3091.2004.00682.x

Hohenegger J (2000) Coenoclines of larger foraminifera. Micropalaeontol 4:127–151

Jacka AD, Brand JP (1977) Biofacies and development and differential occlusion of porosity in a lower Cretaceous (Edwards) reef. J Sed Res 47:366–381. https://doi.org/10.1306/212F7176-2B24-11D7-8648000102C1865D

James NP (1997) The cool-water carbonate depositional realm. In: James NP, Clarke JAD (eds) Cool-water carbonates. Spec Publ Soc Sediment Geol, Berlin

Johnson CC (1999) Evolution of Cretaceous surface current circulation patterns, Caribbean and Gulf of Mexico. In: Barrera E, Johnson CC (eds) Evolution of the Cretaceous ocean-climate system. Geol Soc Am, Berlin

Kämpf J, Sadrinasab M (2006) The circulation of the Persian Gulf: a numerical study. Ocean Sci 2:1–15. https://doi.org/10.5194/os-2-27-2006

Klappa CF (1980) Rhizoliths in terrestrial carbonates: classification, recognition, genesis and significance. Sedimentology 27:613–629. https://doi.org/10.1111/j.1365-3091.1980.tb01651.x

Kutzbach JE, Guetter PJ, Washington WM (1990) Simulated circulation of an idealized ocean for Pangaean time. Palaeoceanography 5:299–317. https://doi.org/10.1029/PA005i003p00299

Lamolda MA, Hancock JM (1996) The Santonian Stage and substages. In: Rawson PF, Dhondt AV, Hancock JM, Kennedy WJ (eds) Proceedings Second International Symposium on Cretaceous Stage Boundaries. Brussels 8–16 September, 1995. Bulletin de l'Institut Royal des Sciences Naturelles de Belgique, Sciences de la Terre, v. 66-suppl.:95–102.

MacEachern JA, Raychaudhuri I, Pemberton SG (1992) Stratigraphic applications of the Glossifungites ichnofacies; delineating discontinuities in the rock record. In Pemberton SG (ed) Applications of Ichnology to Petroleum Exploration; a Core Workshop. SEPM, Core Workshop 16:169–198. https://doi.org/10.2110/cor.92.01.0169

Mangano MG, Buatois LA (1991) Discontinuity surfaces in the Lower Cretaceous of the High Andes (Mendoza, Argentina): Trace

fossils and environmental implications. J South Am Earth Sci 4:215–229. https://doi.org/10.1016/0895-9811(91)90032-G
Martín-Chivelet J, Floquet M, García-Senz J, Callapez PM, López-Mir B, Muñoz JA, Barroso-Barcenilla F, Segura M, Ferreira Soares A, Morgado Dinis P, Fonseca Marques J, Arbués P (2019) Late Cretaceous Post-Rift to Convergence in Iberia. In: Quesada C, Oliveira J (eds) The Geology of Iberia: A Geodynamic Approach Regional Geology Reviews. Springer, Cambridge
McNeill DF, Cunningham KJ, Guertin LA, Anselmetti FS (2004) Depositional themes of mixed carbonate-siliciclastics in the south Florida Neogene: application to ancient deposits. In: Integration of outcrop and modern analogs in reservoir modeling. AAPG Mem 80:23–43.
Michel J, Borgomano J, Reijmer JJG (2018) Heterozoan carbonates: When, where and why? A synthesis on parameters controlling carbonate production and occurrences. Earth-Sci Rev 182:50–67. https://doi.org/10.1016/j.earscirev.2018.05.003
Moro A (1997) Stratigraphy and palaeoenvironments of rudist biostromes in the Upper Cretaceous (Turonian–upper Santonian) limestones of southern Istria, Croatia. Palaeogeogr Palaeoclimatol Palaeoecol 131:13–131. https://doi.org/10.1016/S0031-0182(96)00144-7
Myrow PM (1995) Thalassinoides and the enigma of early palaeozoic open-framework burrow-systems. Palaios 10:58–74. https://doi.org/10.2307/3515007
Myrow PM, Fischer W, Goodge JW (2002) Wave-modified turbidites: combined-flow shoreline and shelf deposits, cambrian, central transantarctic mountains. J Sed Res 72:641–656. https://doi.org/10.1306/022102720641
Niebuhr B, Wilmsen M, Chellouche P, Richardt N, Pürner T (2011) Stratigraphy and facies of the turonian (upper cretaceous) roding formation at the southwestern margin of the bohemian massif (Southern Germany, Bavaria). Z Dt Ges Geowiss 162:294–315. https://doi.org/10.1127/1860-1804/2011/0162-0295
Pemberton SG, MacEachern JA, Dashtgard SE, Bann KL, Gingras MK, Zonneveld J-P (2012) Shorefaces. Develop Sedimentol 64:563–603. https://doi.org/10.1016/B978-0-444-53813-0.00019-8
Pettijohn FJ, Potter PE, Siever R (1987) Sand and Sandstone, 2nd edn. Springer-Verlag, Berlin
Philip JM, Gari J (2005) Late Cretaceous heterozoan carbonates: palaeoenvironmental setting, relationships with rudist carbonates (Provence, south-east France). Sed Geol 175:315–337. https://doi.org/10.1016/j.sedgeo.2004.11.006
Porębski SJ, Steel RJ (2006) Deltas and sea-level change. J Sed Res 76:390–403. https://doi.org/10.2110/jsr.2006.034
Poulain PM (2001) Adriatic Sea surface circulation as derived from drifter data between 1990 and 1999. J Ma Syst 29:3–32. https://doi.org/10.1016/S0924-7963(01)00007-0
Poulsen CJ, Seidov D, Barron EJ, Peterson WH (1998) The impact of palaeogeographic evolution on the surface oceanic circulation and the marine environment within the mid-Cretaceous Tethys. Palaeoceanography 13:546–559. https://doi.org/10.1029/98PA01789
Powell JH, Moh'd BK (2011) Evolution of Cretaceous to Eocene alluvial and carbonate platform sequences in central and south Jordan. GeoArabia 16:29–82. https://doi.org/10.2113/geoarabia160429
Pucéat E, Lécuyer C, Reisberg L (2005) Neodymium isotope evolution of NW Tethyan upper ocean waters throughout the cretaceous. Earth Planet Sci Lett 236:705–720. https://doi.org/10.1016/j.epsl.2005.03.015
Read JF (1985) Carbonate platform facies models. AAPG Bull 66:860–878. https://doi.org/10.1306/AD461B79-16F7-11D7-8645000102C1865D
Read JF (1998) Phanerozoic carbonate ramps from greenhouse, transitional and ice-house worlds: clues from field and modeling studies. In: Wright VP, Burchette TP (eds) Carbonate ramps. Geol Soc, London
Reiss Z, Hottinger L (1984) The Gulf of Aqaba: ecological micropalaeontology. Ecol Studies. Springer-Verlag, Berlin
Rodríguez-Tovar FJ, Puga-Bernabéu Á, Buatois LA (2008) Large burrow systems in marine miocene deposits of the betic Cordillera (Southeast Spain). Palaeogeogr Palaeoclimatol Palaeoecol 268:19–25. https://doi.org/10.1016/j.palaeo.2008.07.022
Romero J, Caus E, Rosell J (2002) A model for the palaeoenvironmental distribution of larger foraminifera based on late middle eocene deposits on the margin of the south pyrenean basin (NE Spain). Palaeogeogr Palaeoclimatol Palaeoecol 179:43–56. https://doi.org/10.1016/S0031-0182(01)00406-0
Sanders D (1996) Rudist biostromes on the margin of an isolated carbonate platform: the upper cretaceous of montagna della maiella, Italy. Eclogae Geol Helv 89:845–871
Sanders D, Pons JM (1999) Rudist formations in mixed siliciclastic–carbonate depositional environments, Upper Cretaceous, Austria: stratigraphy, sedimentology, and models of development. Palaeogeogr, Palaeoclimatol, Palaeoecol 148:249–284. https://doi.org/10.1016/S0031-0182(98)00186-2
Sarkar S, Chakraborty N, Mandal A, Banerjee S, Bose PK (2014) Siliciclastic-carbonate mixing modes in the river-mouth bar palaeogeography of the Upper Cretaceous Garudamangalam Sandstone (Ariyalur, India). J Palaeogeography 3:233–256. https://doi.org/10.3724/SP.J.1261.2014.00054
Schlager W (1991) Depositional bias and environmental change important factors in sequence stratigraphy. Sed Geol 70:109–130. https://doi.org/10.1016/0037-0738(91)90138-4
Schlager W (2005) Carbonate Sedimentology and Sequence Stratigraphy. SEPM, Tulsa
Schwarz E, Veiga GD, Trentini GÁ, Spalletti LA (2016) Climatically versus eustatically controlled, sediment-supply-driven cycles: Carbonate–siliciclastic, high-frequency sequences in the Valanginian of the Neuquén Basin (Argentina). J Sed Res 86(4):312–335. https://doi.org/10.2110/jsr.2016.21
Segura M, García A, Carenas B, García-Hidalgo JF, Gil J (2002) Upper Cretaceous of the Iberian Basin. In: Gibbons W, Moreno T (eds) The Geology of Spain. Geological Society, London
Segura M, Barroso-Barcenilla F, Callapez PM, García-Hidalgo JF, Gil-Gil J (2014) Depositional sequences and ammonoid assemblages in the Upper Cenomanian-Lower Santonian of the Iberian Peninsula (Spain and Portugal). Geológica Acta 12:19–27. https://doi.org/10.1344/105.000002056
Seidler L, Steel R (2001) Pinch-out style and position of tidally influenced strata in a regressive–transgressive wave-dominated deltaic sandbody, Twentymile Sandstone, Mesaverde Group, NW Colorado. Sedimentol 48:399–414. https://doi.org/10.1046/j.1365-3091.2001.00370.x
Seilacher A (1967) Bathymetry and trace fossils. Mar Geol 5:413–428. https://doi.org/10.1016/0025-3227(67)90051-5
Seilacher A (1984) Constructional morphology of bivalves: evolutionary pathways in primary versus secondary soft-bottom dwellers. Palaeontology 27:207–237
Southgate PN, Kennard JM, Jackson MJ, O'Brien PE, Sexton MJ (1993) Reciprocal lowstand clastic and highstand carbonate sedimentation, subsurface Devonian Reef Complex, Canning Basin, Western Australia. In: Loucks RG, Sarg JF (eds) Carbonate Sequence Stratigraphy. AAPG Berlin
Srivastava V, Singh B (2017) Facies analysis and depositional environments of the early Eocene Naredi Formation (Nareda locality), Kutch, Western India. Carbonates Evaporites 32:279–293. https://doi.org/10.1007/s13146-016-0293-6

Steuber T (1996) Stable isotope sclerochronology of rudist bivalves: growth rates and Late Cretaceous seasonality. Geology 24:315–318. https://doi.org/10.1130/0091-7613(1996)024%3C0315:sisorb%3E2.3.co;2

Tänavsuu-Milkeviciene K, Plink-Björklund P, Kirsimäe K, Ainsaar L (2009) Coeval versus reciprocal mixed carbonate–siliciclastic deposition, Middle Devonian Baltic Basin, Eastern Europe: implications from the regional tectonic development. Seminentology 56(5):1250–1274. https://doi.org/10.1111/j.1365-3091.2008.01032.x

Tucker ME (2003) Mixed clastic-carbonate cycles and sequences: quaternary of Egypt and carboniferous of England. Geol Croatica 56(1):19–37. https://doi.org/10.4154/GC.2003.02

Tucker ME, Wright VP (1990) Carbonate sedimentology. Blackwell, London

Ulicny D, Laurin J, Cech S (2009) Controls on clastic sequence geometries in a shallow-marine, transtensional basin: the Bohemian Cretaceous Basin, Czech Republic. Sedimentology 56:1077–1114. https://doi.org/10.1111/j.1365-3091.2008.01021.x

Val J, Aurell M, Badenas B, Castanera D, Subias S (2019) Cyclic carbonate–siliciclastic sedimentation in a shallow marine to coastal environment (latest Kimmeridgian–early Tithonian, Galve subbasin, Spain). J Iber Geol 45:195–222. https://doi.org/10.1007/s41513-018-00098-1

Villalonga R, Boix C, Frijia G, Parente M, Bernaus JM, Caus E (2019) Larger foraminifera and strontium isotope stratigraphy of middle Campanian shallow-water lagoonal facies of the Pyrenean Basin (NE Spain). Facies 65:29. https://doi.org/10.1007/s10347-019-0569-0

Wilmsen M, Fürsich FT, Seyed-Emami K, Majidifard MR, Zamani-Pedram M (2010) Facies analysis of a large-scale Jurassic shelf-lagoon: the Kamar-e-Mehdi Formation of east-central Iran. Facies 56:59–87. https://doi.org/10.1007/s10347-009-0190-8

Wright VP (1994) Palaeosols in shallow marine carbonate sequences. Earth Sci Rev 35:367–395. https://doi.org/10.1016/0012-8252(94)90002-7

Wright LD, Boon JD, Kim SC, List JH (1991) Modes of cross-shore sediment transport on the shoreface of the Middle Atlantic Bight. Mar Geol 96:19–51. https://doi.org/10.1016/0025-3227(91)90200-N

Zhang K-J, Xia B-D, Wang G-M, Li Y-T, Ye H-F (2004) Early cretaceous stratigraphy, depositional environments, sandstone provenance, and tectonic setting of central Tibet, western China. Geol Soc Am Bull 116:1202–1222. https://doi.org/10.1130/B25388.1